Vol. 739: 85–109, 2024
https://doi.org/10.3354/meps14611

MARINE ECOLOGY PROGRESS SERIES
Mar Ecol Prog Ser

Published July 4

Genetic connectivity and isotopic niches of alvinocaridid shrimps from chemosynthetic habitats in Aotearoa/New Zealand, with a new *Alvinocaris* species

Pierre Methou[1,2,*], Nanako O. Ogawa[3], Hidetaka Nomaki[1], Naohiko Ohkouchi[3], Chong Chen[1], Kareen Schnabel[4]

[1]X-STAR, Japan Agency for Marine-Earth Science and Technology (JAMSTEC), Yokosuka, Kanagawa 237-0061, Japan
[2]Univ Brest, Ifremer, CNRS, Unité Biologie des Environnements Extrêmes marins Profonds, Plouzané 29280, France
[3]Biogeochemistry Research Center (BGC), Japan Agency for Marine-Earth Science and Technology (JAMSTEC), Yokosuka 237-0061, Japan
[4]National Institute of Water and Atmospheric Research (NIWA), Wellington 6021, New Zealand

ABSTRACT: Chemosynthetic ecosystems off Aotearoa/New Zealand comprise both hydrothermal vents on the Kermadec Arc and methane seeps on the Hikurangi Margin which host rich communities of specialized fauna including 4 alvinocaridid shrimp species. The systematic positions of these New Zealand alvinocaridid shrimps have not been studied using genetic tools and little is known about their habitat use and feeding habits. Here, we re-evaluate the taxonomy of alvinocaridid shrimps from New Zealand using genetic barcoding and characterize their connectivity and isotopic niches across 8 localities. We describe a new species, *Alvinocaris webberi* sp. nov., previously confused with *A. longirostris*. We also show that *A. alexander* and *A. chelys* are junior synonyms of *A. dissimilis*, revealing a high genetic connectivity across hydrothermal vents and methane seeps from Japan to New Zealand, greatly extending its range. Finally, we find clear niche separation in co-occurring alvinocaridid shrimps, suggesting different diets and/or habitat use. Nevertheless, all species rely on chemosynthetic resources, regardless of the habitat depth, which ranges from 380 to 1650 m.

KEY WORDS: Alvinocarididae · Chemosynthesis · Connectivity · Stable isotope · Hydrothermal vent · Hydrocarbon seep · Methane seep

1. INTRODUCTION

Sustained by microbial chemosynthesis, hydrothermal vents and hydrocarbon seeps host dense biological communities on the deep-sea floor (Levin et al. 2016). These ecosystems constitute spatially restricted assemblages of high biomass and endemicity — but low species diversity — around emissions of geofluids and/or gas (Van Dover & Trask 2000, Levin et al. 2016). Vents and seeps also provide geographically isolated habitats with variations in species composition across different regions constituting distinct biogeographic provinces across the world (Moalic et al. 2012, Rogers et al. 2012, Zhou et al. 2022). This heterogeneous distribution of species results from dispersal barriers related to currents, bathymetry or topography, which limit their ability to reach and connect with other chemosynthetic sites (Adams et al. 2012, Levin et al. 2016). Additionally, a variety of larval developmental modes and dispersal durations (mostly larval dispersal, although adult migration is possible in some highly mobile groups) also affect their distributional ranges and connectivity patterns. Although most vent- and seep-endemic species are limited to one biogeographic province, several examples of species with wider distributions across several

*Corresponding author: pmethou@ifremer.fr

vent or seep biogeographic regions exist (Borda et al. 2013, Tunnicliffe & Breusing 2022, Zhou et al. 2022, Portanier et al. 2023). Distribution in both vent and seep or even organic-fall habitats have also been reported in several groups, including alvinocaridid shrimps (Teixeira et al. 2013, Pereira et al. 2020, He et al. 2023, Methou et al. 2023b), bathymodioline mussels (He et al. 2023) and siboglinid tubeworms (McCowin et al. 2019, 2023); an extreme case is the cosmopolitan distribution of the holothurian *Chiridota hydrothermica* (Thomas et al. 2022).

Within the Southwest (SW) Pacific biogeographic province, the Kermadec Arc constitutes a distinct region of hydrothermal vents (250–1800 m depth) with several unique species of bathymodioline mussels (Boschen et al. 2015b), siboglinid tubeworms (Miura & Kojima 2006) and alvinocaridid shrimps (Webber 2004, Ahyong 2009). Nearby methane seeps hosting dense assemblages of chemosynthetic fauna are also known on the Hikurangi Margin off Aotearoa/New Zealand (720–2300 m depth) with evidence of species overlaps with Kermadec vents (Baco et al. 2010, Bowden et al. 2013). Four species of alvinocaridid shrimps have been listed in New Zealand since the presence of this family was first shown by 2 damaged specimens from a rock dredge sample (Wright et al. 1998), identified as *Alvinocaris* cf. *lusca* (Williams & Chace 1982). Following re-sampling at Brothers Seamount and Rumble V about 160 km southwest of it, 2 species, tentatively called *Alvinocaris* sp. A and *Alvinocaris* sp. B, were reported by Webber & Bruce (2002). Subsequently, the former was identified as *A. longirostris* Kikuchi & Ohta, 1995, widely known from the Northwest (NW) Pacific; and the latter was described as a new species, *Alvinocaris niwa* Webber, 2004. Ahyong (2009) proposed that the type series for the latter species in fact represented 2 distinct species, describing *Alvinocaris alexander* Ahyong, 2009 from part of the original paratype series, and reported the presence of a fourth alvinocaridid species, *Nautilocaris saintlaurentae* Komai & Segonzac, 2004 also found on the Tonga Arc and the North Fiji and the Lau Basins in addition to New Zealand vents (Komai & Segonzac 2004, Komai et al. 2016). Unfortunately, representatives of the different alvinocaridid species from New Zealand have not been included in molecular phylogenetic studies such as the one by Vereshchaka et al. (2015), who combined morphological cladistic analyses with available genetic data for the mitochondrial cytochrome oxidase *c* subunit I (COI) and 16S rRNA gene sequences. Similarly, little is known about their habitat use and feeding habits compared to alvinocaridids from the Atlantic (Gebruk et al. 2000, Ponsard et al. 2013, Methou et al. 2020) or other SW Pacific vents (Methou et al. 2023a). Feeding habits of alvinocaridids are diverse, with some species having a purely chemosymbiotic diet and others displaying bacterivorous, detritivorous or mixed diets (Gebruk et al. 2000, Ponsard et al. 2013, Methou et al. 2020, 2023a).

Variable distributional patterns among these species may be partly due to their diversity of habitats across different depth ranges, which is likely linked to different degrees of dependency on chemosynthetic/photosynthetic organic matters. Although organic matter mostly originates from the chemoautotrophy of various microorganisms, input of photosynthetic carbon can also play a significant role, particularly in shallower sites from the upper bathyal zone (Stevens et al. 2015, Levin et al. 2016, Nomaki et al. 2019). In hydrothermal vents, food web structures at sites above 200 m are largely supported by photosynthetic matter (Comeault et al. 2010, Stevens et al. 2015), whereas deeper sites mostly depend on endogenous chemosynthetic production (Comeault et al. 2010, Stevens et al. 2015, Nomaki et al. 2019). In some cases, evidence of mixed-source diets has been found between 200 and 400 m depth (Stevens et al. 2015). A dominant supply of photosynthetic material was also exceptionally observed at the Mohn's Ridge vent in the Arctic Ocean between 550 and 600 m depth; however, no typical vent-endemic fauna were present there (Sweetman et al. 2013). Similarly, significant reliance on photosynthetic sources was found for some meiofaunal groups in vents from the Izu-Ogasawara Arc between 700 and 900 m depth, contrasting with the chemosynthetic diets of macrofaunal groups from the same area (Nomaki et al. 2019).

The study of nutritional sources and trophic interactions in chemosynthetic ecosystems is often inferred from stable isotope ratios of mainly carbon ($\delta^{13}C$), nitrogen ($\delta^{15}N$) and sulphur ($\delta^{34}S$) that provide complementary ecological information. The use of photosynthetic vs. chemosynthetic organic matter is determined by the large differences in $\delta^{34}S$ between vent fluid sulphides (below 10‰) and seawater sulphates (about 16–21‰) (Fry et al. 1983, Reid et al. 2013). Differences in $\delta^{13}C$ are mostly related to the use of distinct carbon fixation pathways by chemoautotrophic microbes, the Calvin–Benson–Bassham (CBB) cycle (−22 to −30‰) or the reductive tricarboxylic acid (rTCA) cycle (2 to −14‰) (Hügler & Sievert 2011), but can be affected by the use of methane as carbon sources (Portail et al. 2018). Variations in $\delta^{15}N$ have generally been used to infer species' trophic position (Minagawa & Wada 1984); however, studies

have revealed it could also be attributed to distinct inorganic nitrogen sources such as nitrates (5–7‰) and ammonium (<0‰) (Lee & Childress 1994, Riekenberg et al. 2016, Methou et al. 2020).

Here, we use a combination of morphological observations, genetic barcoding and stable isotope analyses to re-evaluate the taxonomy of alvinocaridid shrimps from New Zealand and characterize their genetic connectivity as well as their isotopic niches. Our study addresses the following questions: (1) Does genetic barcoding support the current taxonomic classification of *Alvinocaris* shrimps within this region or does the taxonomy need to be revised? (2) How well are the different populations of these species connected among different sites in the SW and NW Pacific? (3) Is chemosynthesis the main primary production source for the nutrition of all of these shrimps regardless of their depth distribution (350–1650 m depth)? (4) Do these species share and use the same resources within their habitat, or do they show differentiation of their ecological niches?

2. MATERIALS AND METHODS

2.1. Animal sampling

Alvinocaridid shrimps were collected between 2004 and 2012 during 6 oceanographic expeditions sampling hydrothermal vents on the Kermadec Arc: TAN0411, TAN1206, TAN1213, KOK0506, KOK0507 and YK04-09; and 2 expeditions in 2019 (TAN1904) and 2021 (TAN2102) at methane seeps on the Hikurangi Margin (Fig. 1A–C). A total of 95 individuals were sampled using either an epibenthic sledge onboard the research vessel (RV) 'Tangaroa' or a suction sampler mounted on the human-occupied vehicle (HOV) 'Shinkai 6500' onboard the RV 'Yokosuka' (YK04-09), the HOV 'Pisces V' onboard RV 'Ka'imikai-o-Kanaloa' or the remotely operated vehicle (ROV) 'ROPOS' onboard the RV 'Tangaroa'. For comparative purposes, 11 additional shrimp specimens were also collected in 2021 and 2022 on the Higashi-Aogashima vent field (Iizasa et al. 2019) of the Izu-Ogasawara Arc with the suction sampler of the HOV 'Shinkai 6500' (RV 'Yokosuka'; expedition YK22-05) or the ROV 'Hyper-Dolphin' (RV 'Shinsei-Maru'; expedition KS-21-20) (Fig. S1 in Supplement 1 at www.int-res.com/articles/suppl/m739p085_supp1.pdf). For more detailed information on sampling localities and sample processing, see Table S1 in Supplement 2 at www.int-res.com/articles/suppl/m739p085_supp2.xlsx.

2.2. Morphological examination

Size is expressed as postrostral carapace length (CL), excluding rostrum, in mm. Material examined is deposited in the NIWA Invertebrate Collection (NIWA) and the Institute of Marine Biology, National Taiwan Ocean University (NTOU). Individuals were identified as male (M) or female (F) based on sexual dimorphism of the first and second pleopod appendages and position of the gonopores. Ovigerous females (ov.) were identified when brooding eggs under their abdomens, and juveniles (juv.) were small-sized individuals with red/orange lipid stores. All measurements, identification and terminology follow Komai & Segonzac (2005), Webber (2004) and Ahyong (2009). The species description of *Alvinocaris webberi* sp. nov. indicates ranges and measurements across all adult specimens examined, with measurements for the holotype given in square brackets.

2.3. DNA extraction and sequencing

Pieces of abdominal muscle were used to extract DNA from 106 alvinocaridid shrimps using the DNeasy Blood & Tissue kit (Qiagen) and following the manufacturer's instructions. The specific Cari-COI-1F and Cari-COI-1R alvinocaridid primers, designed to avoid amplification of potential mitochondrial pseudogenes, amplified a 734 bp fragment of the COI gene 5′ region (Methou et al. 2020). In addition, for 3 individuals of each species, a 914 bp fragment of the 18S gene and a 715 bp fragment of the 28S gene were amplified with the 18S-1F and 18S-5R primers for 18S and 28S-C1 and 28S-D2 primers for 28S (Aznar-Cormano et al. 2015). These amplifications were done in a 25 µl reaction mixture including 10.5 µl of RNAse-free H_2O, 12.5 µl of 2× Premix ExTaq HS buffer which included dNTPs mix and *Taq* polymerase (TaKaRa Bio), 0.5 µl of each primer at 10 µM, and 1–3 µl of the shrimp template DNA. Conditions for PCR cycling followed Methou et al. (2023b), with 35 cycles at 50°C as the annealing temperature for COI, 40 cycles at 51°C for 18S and 40 cycles at 55°C for 28S. Sanger sequencing of these PCR products was conducted on both strands by the FASMAC Corporation (Kanagawa, Japan). Sequence editing of forward and reverse strands was performed using Geneious Prime® 2023.1.2 (https://www.geneious.com). Phylogenetic trees were constructed using the MrBayes plugin v3.2.6 (Huelsenbeck & Ronquist 2001) in the Geneious software. New sequences generated in this

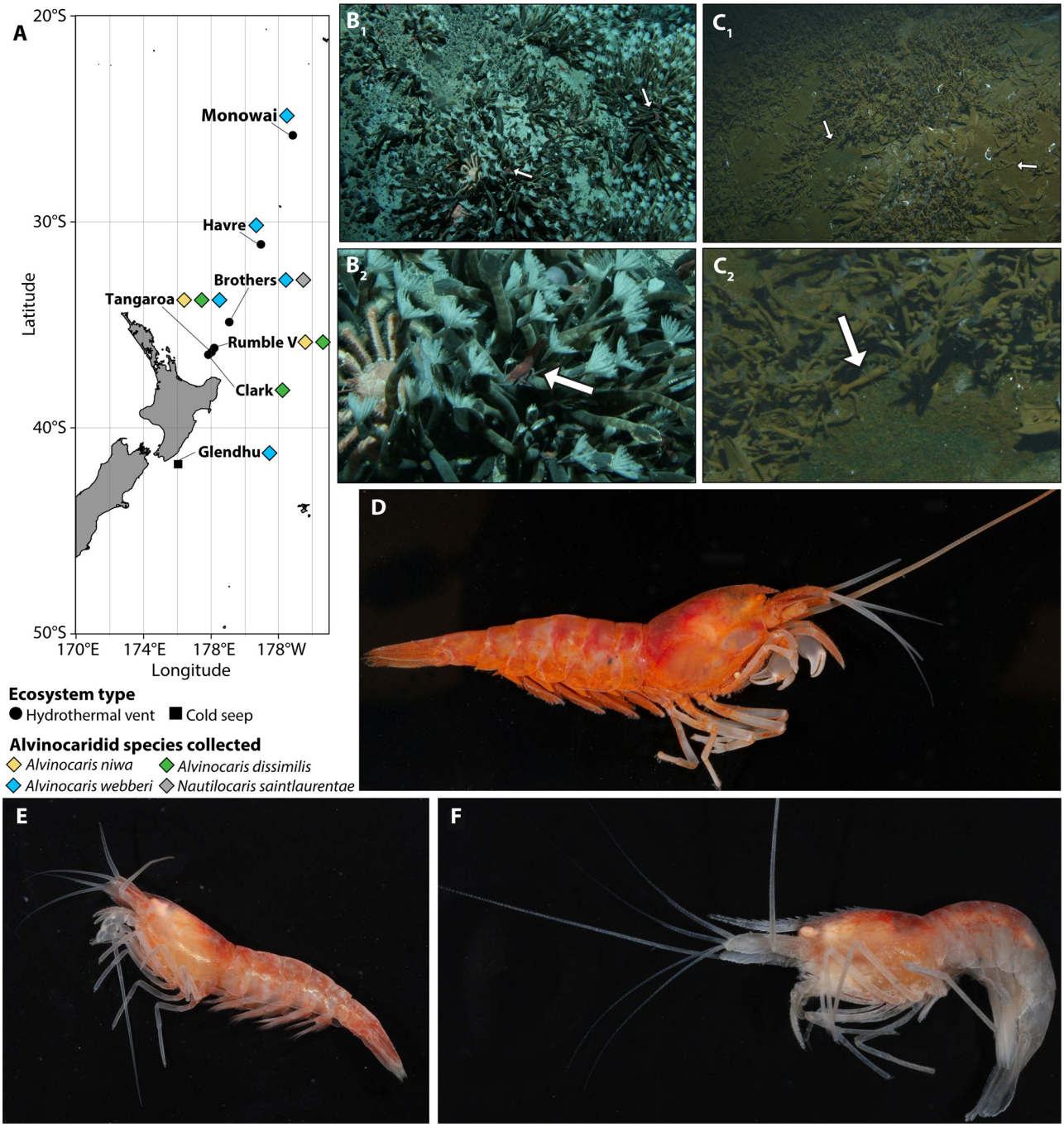

Fig. 1. (A) Geographical context of alvinocaridid shrimps from chemosynthetic ecosystems in Aotearoa/New Zealand. (B) Chemosynthetic communities of stalked barnacles at Brothers Seamount hosting alvinocaridid shrimps (indicated by white arrows). (C) Chemosynthetic communities of stalked barnacles and *Bathymodiolus* mussels at Tangaroa Seamount hosting alvinocaridid shrimps (indicated by white arrows). (D) Specimen of *Alvinocaris niwa* collected at the summit of Tangaroa Seamount. (E) Specimen of *A. dissimilis* (formerly *A. alexander*) from Rumble V Seamount (eastern flank). (F) Specimen of *A. webberi* sp. nov. from Brothers Seamount

study are deposited in NCBI GenBank under accession numbers OR750757–OR750768; OR750745–OR750756; OR734008–OR734016; and OR766468–OR766495. Additional sequences from Methou et al. (2023b) were also used (see Table S1 for specimen details). Details of haplotypes are given in Table S2 in Supplement 1 (also see Supplement 1 for all following supplemental tables and figures).

2.4. Population genetics analyses

Haplotype networks were built on a 734 bp alignment of the COI gene using the median-joining algorithm (Bandelt et al. 1999) implemented in PopART v1.7 (Leigh & Bryant 2015) with the epsilon parameter set to 0. The same alignment was used to detect barcode gaps with the Assemble-Species-by-Automatic-Partitioning (ASAP) method developed by Puillandre et al. (2021) to identify the most probable partitioning of species-level clades in the *A. dissimilis* species complex.

Number of variable sites (S), haplotype diversities (H_d), nucleotide diversities (π) and average number of nucleotide differences (k) (Tajima 1983) of each shrimp species and population were inferred using DnaSP v6 (Rozas et al. 2017). Using the same software, net genetic distances (D_a) were calculated from haplotype frequencies among each local population. For all shrimp species, Tajima's D and Fu and Li's F-statistics (Fu & Li 1993) were computed to test the hypothesis of demographic changes against the null hypothesis of a mutation-drift equilibrium. Finally, analysis of molecular variance (AMOVA) and pairwise F_{ST} with 1000 permutations were calculated among populations defined in DnaSP, using Arlequin v3.5.2.2 (Excoffier et al. 1992).

2.5. Stable isotope measurements and analyses

Abdominal muscles were dissected from each individual, oven-dried to constant mass at 60°C for more than 48 h and then ground into powder using a mortar and pestle. Mortar, pestle and handling tools were cleaned with ethanol and chloroform between each sample to remove residual traces of lipids. The pretreated muscle powder was transferred quantitatively to a precleaned tin foil capsule for the isotope analysis described below.

Carbon and nitrogen stable isotope compositions were determined by a nano-elemental analyser–isotope ratio mass spectrometer (nano EA/IRMS) system consisting of a modified elemental analyzer (Flash EA1112, Thermo Finnigan, Bremen, Germany), continuous flow interface (ConFlo III, Thermo Finnigan) and an isotope ratio mass spectrometer (Delta plus XP, Thermo Finnigan; Ogawa et al. 2010, Isaji et al. 2020). Sulphur isotopic compositions were determined by a nano EA/IRMS for S system with a modified elemental analyser (Flash 2000, Thermo Scientific), gas chromatography (GC-2010 Plus, Shimadzu), a ConFlo III and a Delta plus XP IRMS. The carbon, nitrogen and sulphur isotopic compositions are expressed in conventional δ notation relative to Vienna Pee Dee belemnite, air and Vienna–Canyon Diablo troilite.

The isotopic compositions were calibrated using inter-laboratory determined standards ranging from −26.86 to 0.18‰ for $\delta^{13}C$ and from −5.73 to 60.40‰ for $\delta^{15}N$ (L-tyrosine, L-alanine, L-proline, L-valine, L-glutamic acid; Tayasu et al. 2011, Sun et al. 2023). Authentic international standards ranging from −34.1 to 21.17‰ (IAEA-SO-5, IAEA-SO-6 and NBS127) were used for the $\delta^{34}S$ calibration. The analytical uncertainties determined based on replicate measurements of L-tyrosine (for $\delta^{13}C$ and $\delta^{15}N$) and NBS127 (for $\delta^{34}S$) were smaller than ±0.3‰ for $\delta^{13}C$, ±0.2‰ for $\delta^{15}N$ and ±0.5‰ for $\delta^{34}S$ (1σ).

For each individual, isotopic datasets were grouped by species and localities. Statistical comparisons of $\delta^{13}C$, $\delta^{15}N$ and $\delta^{34}S$ among groups were carried out with the non-parametric Kruskal-Wallis test followed by post hoc Dunn tests (detailed p-values of these tests are given in Table S3). All analyses were performed in the R v4.2.1 statistical environment. In addition, the 'Stable Isotope Bayesian Ellipses in R (SIBER)' v2.1.6 package (using the unit $‰^2$ for ellipse areas introduced by Jackson et al. 2011) was used to explore isotopic niches of shrimp species as a proxy of their realized ecological niches since variations in the isotopic composition of animals are dictated by both their habitat use (Flaherty & Ben-David 2010) and the prey items consumed (McCutchan et al. 2003, Jackson et al. 2011). For each population, standard ellipses were constructed in 2 separated sets: one with $\delta^{13}C$ and $\delta^{15}N$ data and another with $\delta^{13}C$ and $\delta^{34}S$ data. Overlaps between these standard ellipses were interpreted as partial sharing of food sources and/or habitat resources between groups, with more sharing resulting in larger overlap (Jackson et al. 2011).

3. RESULTS

3.1. Morphometric analysis

Table 1 provides key comparative morphometrics for the 4 putative species (*Alvinocaris dissimilis*, *A. alexander*, *A. chelys* and *A. stactophila*) using those characters typically used to discriminate species of *Alvinocaris* (Komai & Segonzac 2005; for a comprehensive list of morphometric characters, see Table S4). The differences between the former 3 species are slight and overlap in nearly all regards, with the exception of the rostral length, which appears to be slightly longer in *A. dissimilis* (0.53–0.61 × CL,

Table 1. Morphological characteristics of 4 taxa in the *Alvinocaris dissimilis* complex: *A. dissimilis* Komai & Segonzac, 2005, *A. alexander* Ahyong, 2009, *A. chelys* Komai & Chan, 2010 and *A. stactophila* Williams, 1988. Grey boxes highlight key morphological differences between the putative species. Characters and terminology follow Komai & Segonzac (2005). CL: carapace length. For full list of comparative morphological characters, see Table S4 in Supplement 1

Morphological character	Species			
	A. dissimilis	*A. alexander*	*A. chelys*	*A. stactophila*
Carapace: dorsal angle (°)	155	145	155	**170**
Rostrum: length (× CL)	**0.53–0.61 Usually reaching to A2 to slightly overreaching**	0.25–0.39 Not reaching mid-length of A2	0.28–0.45 Not reaching end of A2 (reaching end of A1 to mid-length of A2)	0.42 Not reaching end of A2 (slightly overreaching A1)
Telson: posterior margin spines	2 pairs of posterolateral spines, plumose setae	2 pairs of posterolateral spines, plumose setae	2 pairs of posterolateral spines, plumose setae	**8 pairs of spines; longest pair (2nd pair) distinctly curved**
Pereopod 3: spines on dactylus	Distal-most accessory spine large, proximally declining in size	Distal-most accessory spine large, proximally declining in size	Distal-most accessory spine large, proximally declining in size	**Distal 4 accessory spines subequal in size, larger than distal-most spine**

compared to 0.25–0.45 × CL for both *A. alexander* and *A. chelys*), with the rostrum usually reaching to slightly overreaching the second antennular peduncle, compared to not reaching the mid-length in both *A. alexander* and *A. chelys* (Table 1). Additional material for *A. alexander* could extend some of the ranges deemed as diagnostic characters by Ahyong (2009), e.g. the antennal scale can be up to twice as long as broad (1.90–2.16 in *A. dissimilis*), the telson length:width ratios overlap with those of both *A. dissimilis* and *A. chelys*, and the length:width ratios of the second antennular peduncle overlap, with ratios of 1.3–1.4 for *A. alexander*, 1.3–1.7 for *A. chelys* and 1.4–1.8 for *A. dissimilis*. Furthermore, the proposed character of the extent of the postrostral ridge (posterior two-thirds or beyond for *A. alexander* and mid-length for *A. dissimilis*) is variable in the specimens examined, e.g. the ridge only reaches to mid-length in a large male (NIWA 86458, see Section 5).

In contrast, *A. stactophila* is only known from seeps in the Gulf of Mexico, with unusual apomorphic characters such as the spination of the telson; *A. stactophila* has 8 pairs of spines, with the lateral pair conspicuously long and curved, while the other species have only plumose setae along the distal margin of the telson; the spination of the third pereopod is unusual, with the distal 4 accessory spines subequal in size, compared to proximally declining in size in the other species.

Alvinocaris niwa displays a number of unique characters, as also reported by Webber (2004): the row of spines along the lateral margin of the distal segment of the third maxilliped is apomorphic within the Alvinocarididae; a number of distal spines are usually present in other species, but the lateral face is smooth or only furnished with a few stiff setae. The shape of the mandibular incisor process differs slightly, with the distal half slightly set back from the proximal half and formed by a row of 3 to 4 teeth, rather than a single tooth as appears to be most common for other species in this family (Fig. 2). This character is not always illustrated for all species, and the stability of this character is not reportedbterminal rows of spines are shared with the clade of species containing *Rimicaris* Williams & Rona, 1986 and the former genera *Opaepele* Williams & Dobbs, 1995, *Manuscaris* Komai & Tsuchida, 2015 and *Alvinocaridinides* Komai & Chan, 2010 which have been recently synonymized under *Rimicaris* (Methou et al. 2024). The former genus *Shinkaicaris* Komai & Segonzac, 2005, now also synonymized under *Rimicaris* (Methou et al. 2024), displays 3 or 4 rows of spines. This differs from nearly all *Alvinocaris*, with only *A. komaii* Zelnio & Hourdez, 2009 displaying this character, although it is variable (the holotype only has a single row of spines along the dactylar flexor margin).

3.2. Phylogeny, haplotype networks and genetic diversities

Phylogenetic reconstruction using the COI gene indicates that shrimps from the Kermadec Arc previously identified as *A. longirostris* were in fact closer to *A. muricola* from the Atlantic, the two in turn being sister to the clade comprising *A. longirostris* and *A.*

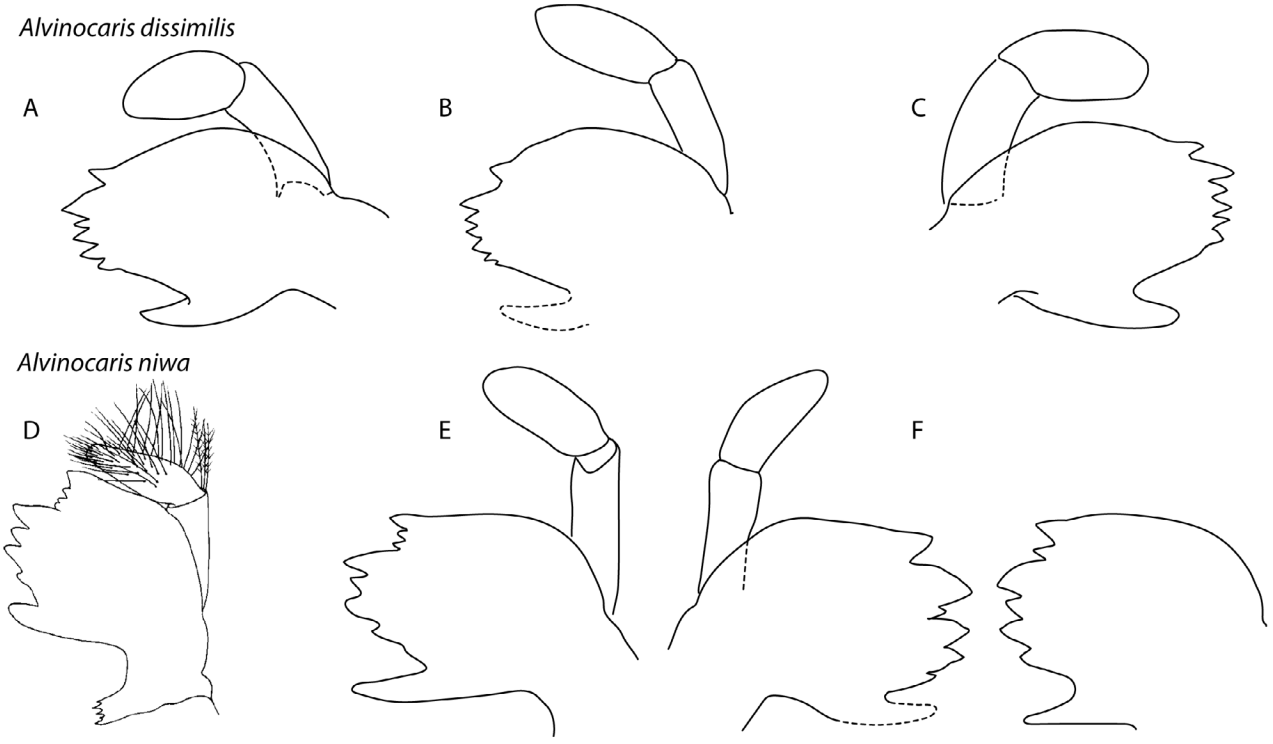

Fig. 2. Mandible, posterior (convex) view. (A–C) *Alvinocaris dissimilis* Komai & Segonzac, 2005. (D–F) *Alvinocaris niwa* Webber, 2004. (A) female, NIWA 42014, carapace length (CL) 9.7 mm (*A. alexander* paratype). (B) Male, NIWA 86458, CL 8.2 mm. (C) Ovigerous female, NIWA 82323, CL 10.9 mm. (D) Holotype male, NIWA 3253, CL 15.4 mm (reproduced from Webber 2004). (E) Male, NIWA 32842, CL 14.0 mm. (F) Male, NIWA 32842, CL 12.3 mm

lusca with strong support from posterior probabilities (Fig. 3A). These individuals represent a new *Alvinocaris* species, named *Alvinocaris webberi* sp. nov. herein (see Section 5 for a detailed description). This phylogenetic tree also shows that *A. dissimilis* and its junior synonyms *A. chelys* and *A. alexander* formed a clade together with *A. stactophila*, sister to most *Alvinocaris* species, including *A. kexueae, A. solitaire*, and those mentioned above (Fig. 3A). A similar clade grouping *A. dissimilis* with *A. chelys* and *A. alexander* was also obtained with a concatenated phylogeny of the 18S and 28S genes, but sister to all *Alvinocaris* and *Rimicaris* species (Fig. 3B). *A. niwa* is recovered sister to the *Rimicaris* clade, with high posterior probability in the COI phylogeny (Fig. 3A) and sister to a clade formed by *A. longirostris*, *A. lusca* and *A. webberi* sp. nov. on the concatenated 18S–28S phylogeny and with very low posterior probability (Fig. 3B). The lower resolution on the nuclear tree could be explained by low taxon sampling, with only a small number of alvinocaridid species with 18S and 28S genes available in online databases, and because these markers are more conservative.

Specimens initially identified as *A. dissimilis*, *A. chelys* and *A. alexander* constituted a network of 11 haplotypes, with 2 haplotypes shared among the 3 species, out of 45 barcoded individuals, including sequences from Yahagi et al. (2015) for *A. dissimilis* from Minami-Ensei and from Vereshchaka et al. (2015) for *A. chelys* from Gueishandao (also known as Kueishan Island) (Fig. 4A). These 3 species are now all synonymized under *A. dissimilis* (see 'Systematics', Section 5). For *A. niwa* and *A. webberi* sp. nov., 7 and 10 haplotypes were identified out of 24 and 42 barcoded individuals, respectively (Fig. 4B,C). The number of variable sites (S) was 7, 10 and 11, respectively, for *A. niwa*, *A. webberi* sp. nov. and *A. dissimilis*. *A. dissimilis* and *A. webberi* sp. nov. showed comparable haplotype diversities (H_d = 0.495 ± 0.092 and 0.517 ± 0.091, respectively); however, nucleotide diversity (π) was more than twice higher for *A. dissimilis* (Table 2). Haplotype diversity of *A. niwa* (H_d = 0.678 ± 0.090) was slightly higher than for the other 2 alvinocaridids, but nucleotide diversity was slightly lower than in *A. dissimilis* (Table 2). The average number of nucleotide differences (k) was comparable between *A. niwa* and *A. dissimilis* (k = 1.127 and 1.372, respectively) but was lower for *A. webberi* sp. nov. (k = 0.632).

A. niwa and *A. webberi* sp. nov. exhibited no genetic structuring, with all of the variation occurring within

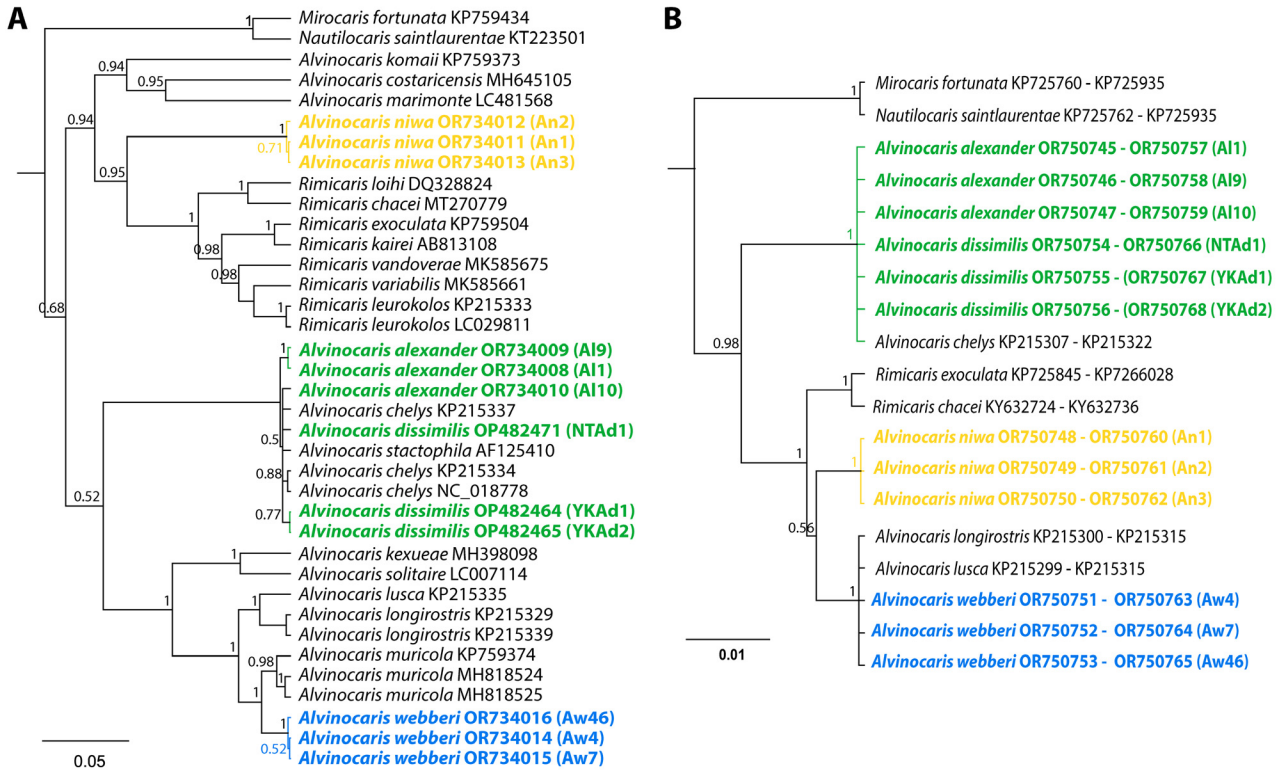

Fig. 3. Phylogenetic tree of alvinocaridid shrimps based on Bayesian inference using a GTR model. Numbers on each node indicate posterior probabilities. New sequences of species from chemosynthetic ecosystems off Aotearoa/New Zealand and the northwestern Pacific are highlighted. (A) Phylogenetic tree using the mitochondrial cytochrome oxidase *c* subunit I (COI) mitochondrial markers. (B) Concatenated tree using the 18S and 28S nuclear markers

their populations (Table 3). Similarly, AMOVAs showed low F_{ST} values (0.0054, p = 0.39) for the *A. dissimilis* species complex, with 99.46% of the genetic variation occurring within populations (Table 3). Net genetic distances (D_a) among local populations were also very low, including among localities from the Okinawa Through, the Izu-Ogasawara Arc and the Kermadec Arc. These ranged from 0.00002 between populations from Minami-Ensei and off-Gueishandao vents and 0.00112 between Higashi-Aogashima and Tangaroa vents (Table S5). Similarly, the 2 best partitions with lowest ASAP score obtained by the barcode gap approach on the *A. dissimilis* complex delimited either 3 or 2 distinct subsets, but none that was statistically supported (p > 0.1; Fig. S2). These partitions did not correspond to a geographical clustering by site nor to a clustering by putative species, with each subset including at least a mix of *A. alexander* and *A. dissimilis* individuals. In addition, the distribution of pairwise differences did not follow any clear patterns (Fig. S2).

Demographic analyses suggested a population expansion of *A. webberi* sp. nov., with significantly negative values for Tajima ($D = -2.019$, $p < 0.05$) and Fu & Li tests ($F = -3.726$, $p < 0.05$). Conversely, populations of *A. niwa* and *A. dissimilis* best fitted a model of constant size populations with Tajima (*A. niwa*: $D = -1.521$, $p > 0.1$; *A. dissimilis*: $D = -1.507$, $p > 0.1$) and Fu & Li values (*A. niwa*: $F = -1.873$, $p > 0.1$; *A. dissimilis*: $F = -1.914$, $p > 0.1$) that were not significantly different from zero.

Combining morphological and genetic evidence, we refer to the alvinocaridid species hereinafter by their revised taxonomy: *A. dissimilis* and *A. webberi* sp. nov. (see Section 5 for additional details).

3.3. Stable isotope analysis

Alvinocaridid shrimps showed significantly distinct $\delta^{13}C$ values among species and among vent fields (Kruskal-Wallis $\chi^2 = 52.46$, $p < 0.001$, df = 8; Fig. 5), with significantly less-negative ^{13}C values for *A. niwa* compared to *A. dissimilis* both at Tangaroa and Rumble V Seamounts (Dunn's multiple comparison tests, $p < 0.001$). On the other hand, no

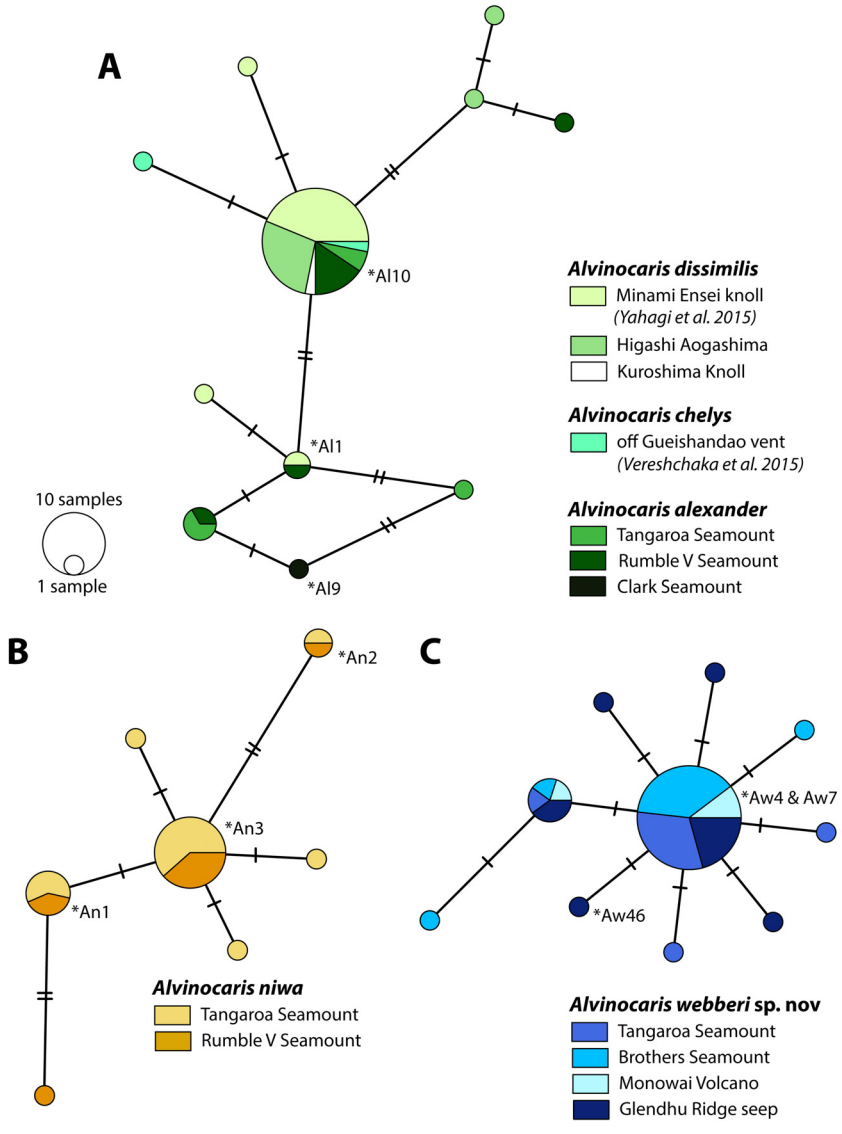

Fig. 4. COI haplotype networks of alvinocaridid shrimps from chemosynthetic ecosystems off Aotearoa/New Zealand and Japan. Names of specimens used for the phylogeny are indicated after an asterisk (*) next to their corresponding haplotype. (A) Haplotype network of specimens of *Alvinocaris dissimilis*, including specimens previously identified as *A. chelys* and *A. alexander* (now junior synonyms). (B) Haplotype network of *A. niwa*. (C) Haplotype network of *A. webberi* sp. nov.

clear variation in $\delta^{13}C$ was found among vent populations of *A. niwa* and *A. dissimilis* (Dunn's multiple comparison tests, $p > 0.05$) but *A. webberi* sp. nov. from Brothers Seamount showed a significant ^{13}C-enrichment compared to those from Tangaroa and Monowai (Dunn's multiple comparison tests, $p < 0.001$; Fig. S3). Marked variations in $\delta^{15}N$ could also be observed among shrimp species (Kruskal-Wallis $\chi^2 = 48.02$, $p < 0.001$, df = 8; Fig. 5), with significantly higher $\delta^{15}N$ values for *A. niwa* compared to the other 2 co-occurring alvinocaridid species at Tangaroa Seamount (Dunn's multiple comparison tests, $p < 0.001$, df = 8; Fig. S4) and slightly higher $\delta^{15}N$ values for *A. niwa* compared to *A. dissimilis* at Rumble V Seamount (Dunn's multiple comparison tests, $p < 0.05$). The 3 *Alvinocaris* species had relatively similar $\delta^{15}N$ values among populations from different vent fields except a slightly higher $\delta^{15}N$ at Rumble V Seamount compared to Higashi-Aogashima for *A. dissimilis* and a slightly lower $\delta^{15}N$ at Tangaroa Seamount compared to Brothers Seamount for *A. webberi* sp. nov. (Dunn's multiple comparison tests, $p < 0.05$; Fig. S3). Variations in $\delta^{34}S$ were also found (Kruskal-Wallis $\chi^2 = 32.69$, $p < 0.001$; Fig. 5), with a ^{34}S-depletion for *A. webberi* sp. nov. from Tangaroa Seamount compared to the other 2 vent fields (Monowai and Brothers) (Dunn's multiple comparison tests, $p < 0.05$) and a ^{34}S-enrichment for *A. dissimilis* from Higashi-Aogashima compared to populations from the Kermadec Arc (Dunn's multiple comparison tests, $p = 0.01$).

Our SIBER analysis revealed that the core isotopic niches of alvinocaridid shrimps were generally well separated among species inhabiting the same vent fields (Fig. 5; Fig. S4). Hence, at Tangaroa Seamount, only a limited overlap of 2.07‰^{2} (i.e. 21.4% of the smaller ellipse area) for carbon versus nitrogen ellipses and of 11.7‰^{2} (i.e. 24% of the smaller ellipse area) for carbon versus sulphur ellipses was found between *A. niwa* and *A. webberi* sp. nov., whereas *A. webberi* sp. nov. and *A. dissimilis* clearly overlapped for carbon versus nitrogen ellipses (3.97‰^{2}; i.e. 55.4% of the smaller ellipse area) but only slightly for carbon versus sulphur ellipses (2.22‰^{2}; i.e. 4.6% of the smaller ellipse area). At Brothers Seamount, a notable overlap of 3.81‰^{2} (i.e. 42.5% of the smaller ellipse area) could be observed between *A. webberi* sp. nov. and *Nautilocaris saintlaurentae* for carbon versus nitrogen ellipses, but no overlap was found for carbon versus sulphur ellipses. Comparison of isotopic niches from

Table 2. Genetic diversity based on partial mitochondrial cytochrome oxidase *c* subunit I (COI) sequences from alvinocaridid shrimps for each species and sampling site. N: number of sequenced individuals for each population; *S*: number of variable sites; *h*: number of haplotypes; H_d: haplotype diversity (±SD); π: nucleotide diversity; *k*: number of nucleotide differences

Species / Population	N	*S*	*h*	H_d	π	*k*
				Statistics		
Alvinocaris niwa						
Tangaroa	15	6	6	0.705 ± 0.114	0.00138	1.010
Rumble V	9	5	4	0.694 ± 0.147	0.00189	1.389
All populations	24	8	7	0.678 ± 0.090	0.00154	1.127
***Alvinocaris dissimilis* complex**						
Gueishandao	2	1	2	1.0 ± 0.500	0.00152	1.000
Minami-Ensei	17	4	4	0.331 ± 0.143	0.00103	0.676
Higashi-Aogashima	12	4	4	0.636 ± 0.128	0.00185	0.836
Tangaroa	5	7	4	0.900 ± 0.161	0.00490	3.600
Rumble V	8	8	5	0.857 ± 0.108	0.00384	2.821
All populations	44	12	11	0.495 ± 0.092	0.00208	1.372
***Alvinocaris webberi* sp. nov.**						
Monowai	4	1	2	0.500 ± 0.265	0.00068	0.500
Brothers	14	3	4	0.396 ± 0.159	0.00075	0.549
Tangaroa	12	3	4	0.455 ± 0.170	0.00068	0.500
Glendhu	12	5	6	0.758 ± 0.122	0.00132	0.970
All populations	42	9	10	0.517 ± 0.091	0.00086	0.632

Table 3. Analyses of molecular variance among sampling sites based on partial COI sequences from 3 alvinocaridid shrimps

Species	F_{ST}	p	Among-population variation (%)	Within population-variation (%)
			Statistics	
Alvinocaris niwa	0	1	0	100
Alvinocaris dissimilis complex	0.0054	0.39	0.54	99.46
Alvinocaris webberi sp. nov.	0	1	0	100

different fields showed distinct trends depending on the species (Fig. 5; Fig. S3). For *A. niwa*, a striking overlap was found between populations from Tangaroa and Rumble V for both carbon versus nitrogen ellipses (5.54‰^{2}; i.e. 72.9% of the smaller ellipse area) and carbon versus sulphur ellipses (14.16‰^{2}; i.e. 85.8% of the smaller ellipse area). On the other hand, niches of the different *A. webberi* sp. nov. populations segregated clearly except between Brothers Seamount and Tangaroa Seamount with a slight overlap of 0.57‰^{2} (i.e. 6.3% of the smaller ellipse area) for carbon versus nitrogen ellipses. For *A. dissimilis*, niches of Tangaroa and Rumble V populations strongly overlapped for carbon versus sulphur ellipses (12.05‰^{2}; i.e. 81.2% of the smaller ellipse area) but were completely separated in terms of carbon versus nitrogen ellipses.

4. DISCUSSION

4.1. Alvinocaridid shrimps from Aotearoa/New Zealand show different distributional ranges

Our taxonomic revision combined with individual barcoding revealed the existence of a new species of *Alvinocaris*, *A. webberi* sp. nov., previously presented as *A. longirostris* (95.1% pairwise identity; partial COI gene) in the absence of genetic data (Webber 2004). In fact, it is genetically closer to *A.* aff. *muricola* (97.5% pairwise identity; partial COI gene) collected on experimental free-fall landers deployed off the Brazilian deep margin in the SW Atlantic (Pereira et al. 2020). This revision also synonymizes *A. alexander* and *A. chelys* with *A. dissimilis*, and for the first time provides DNA sequences for *A. niwa*. The genetic similarity of *A. dissimilis* with *A. stactophila* on the COI marker is surprising and also highlights the need for further taxonomic revisions of this clade. However, the morphological differences of *A. stactophila* in several characters and its extremely distant geographical distribution (Gulf of Mexico), on the other side of the globe, raise caution before including this species into the proposed synonymy of *A. dissimilis*. Without access to *A. stactophila* specimens for our analyses, we believe that future work including additional individuals is required to comprehensively resolve the taxonomy of this group.

These results drastically extend the distribution of *A. dissimilis*, which was previously known only from the Okinawa Trough at the Minami-Ensei Knoll vent field (Komai & Segonzac 2005), recently expanded to the Higashi-Aogashima vent field on the Izu-Bonin Arc and the Kuroshima Knoll methane seep on the Ryukyu Arc (Methou et al. 2023b), and now is known to inhabit 4 additional locations on the Kermadec Arc, namely the Brothers, Tangaroa, Rumble V and Clark Seamounts (Fig. 1; Fig. S1). Thus, *A. dissimilis* exhibits genetic homogeneity in the marker genes used, despite the large geographical distances between sites. Such cases of implied broad-scale genetic connectivity are not uncommon in alvinocaridids, with several examples of panmictic popula-

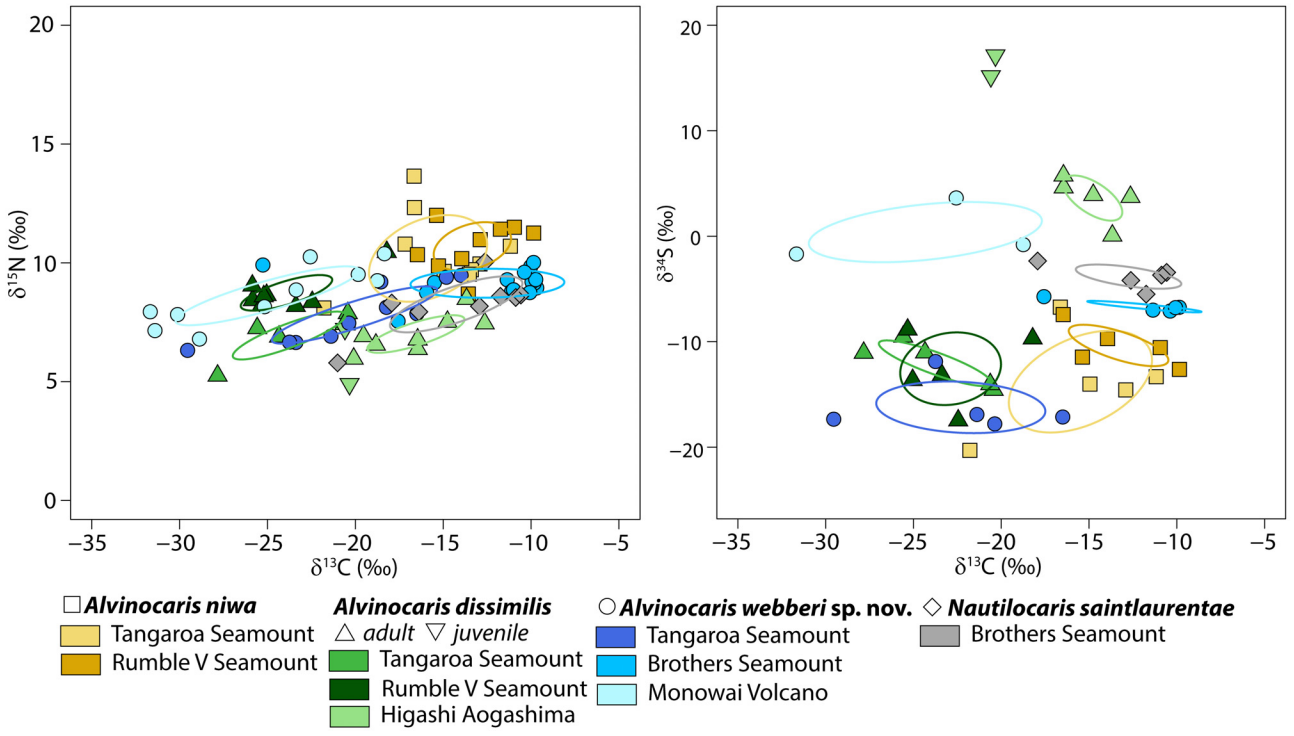

Fig. 5. Comparison of isotopic niches ($\delta^{13}C$ against $\delta^{15}N$ on the left and $\delta^{13}C$ against $\delta^{34}S$ on the right) of *Alvinocaris niwa*, *A. dissimilis*, *A. webberi* sp. nov. and *Nautilocaris saintlaurentae* from different vent fields

tions in *Rimicaris exoculata* or *Alvinocaris markensis* across their entire distribution in the Atlantic Ocean (Teixeira et al. 2012, 2013). Highly connected populations were also reported for *Rimicaris kairei* across distinct biogeographic regions in the Indian Ocean (Zhou et al. 2022). Similarly in the Pacific Ocean, *R. loihi*, previously known as *Opaepele loihi* (Methou et al. 2024), or *A. longirostris* appear to have extended geographical distributions, across the Mariana Arc and Loihi Seamount near Hawaii for *R. loihi* (Stevens et al. 2008) and from Sagami Bay to Okinawa Trough, South China Sea, to the Manus Basin for *A. longirostris* (Yahagi et al. 2015, Van Audenhaege et al. 2019, He et al. 2023). For *A. dissimilis*, no intermediate sites between the SW Pacific (Kermadec Arc, Lau Basin, Hikurangi Margin) and the NW Pacific (Okinawa Trough, Izu-Ogasawara Arc, Sagami Bay) are so far known despite more than 9000 km of distance.

Early larval stages of 4 previously studied alvinocaridid species showed similar morphological characteristics among the different species, suggesting an early lecithotrophic phase followed by an extended development, which are indicative of a long planktonic larval duration and large dispersal potential (Hernández-Ávila et al. 2015). In addition, although the exact position of alvinocaridid larvae in the water column during the dispersal phase is not known for any of these species (Methou et al. 2020), the distribution of *A. dissimilis* in relatively shallow vent fields — up to 380 m depth for Rumble V — suggests a possible enhanced dispersal in shallow and faster oceanic currents, at least for larvae departing from the shallowest sites. *Lamellibrachia columna* tubeworms also offer an interesting case in a similar geographic context to *A. dissimilis*, with evidence of genetic connectivity across methane seeps in Sagami Bay and Nankai Trough off Japan and in the Hikurangi Margin off New Zealand as well as hydrothermal vents of the Lau Basin (McCowin et al. 2019).

Conversely, the other 2 alvinocaridids showed a much more limited distribution, restricted to the Kermadec Arc vents and the Hikurangi Margin seeps for *A. webberi* sp. nov. and to the Kermadec Arc vents only for *A. niwa* (Fig. 1). At present, these 2 species have to be considered endemic and range restricted to those localities, with further sampling of hitherto underexplored chemosynthetic habitats in the region still required. Future work combining a population genomic approach, such as RAD-sequencing, and dispersal simulation modelling could also provide opportunities to assess ongoing connectivity among sites and define which are the source populations of these shrimp species.

4.2. Alvinocaridid shrimps occupy distinct niches within vent fields of the Kermadec Arc

Regardless of the hydrothermal vent field occupied, co-occurring alvinocaridid shrimps on the Kermadec Arc exhibited distinct isotopic niches with little to no overlap, suggesting a different use of their habitat resources. This niche partitioning between *A. niwa* and the other shrimp species was mostly related to ^{13}C- and ^{15}N-enriched sources for *A. niwa*. On the other hand, niches of *A. webberi* sp. nov. and *A. dissimilis* at Tangaroa and niches of *A. webberi* sp. nov. and *Nautilocaris saintlaurentae* at Brothers were segregated mostly by a ^{34}S-depletion for *A. webberi*. The different morphology of *A. niwa* mouthpart appendages, in particular the mandible, compared to *A. webberi* and *A. dissimilis* also support a distinct feeding regime for this species. However, variation in geochemical signatures between the different geographical sites might have also impacted this isotopic niche segregation between the different alvinocaridid species, and this variability must be taken into account to assess niche partitioning between these shrimps (see Section 4.3).

At hydrothermal vents, δ^{13}C variations are mostly attributed to the use of different carbon fixation pathways by the chemosynthetic primary producers, with typical δ^{13}C values of −15 to −10‰ for rTCA-fixing microorganisms and −36 to −30‰ for CBB-fixing ones (Hügler & Sievert 2011, Portail et al. 2018). Alvinocaridid shrimps at Kermadec vent fields were either found directly on rocks close to bacterial mats or within faunal assemblages of the stalked barnacle *Vulcanolepas osheai* (Buckeridge 2000), or the vent mussels *Gigantidas gladius* (Boschen et al. 2015b; Tangaroa and Rumble V) and *Bathymodiolus manusensis* (Leybourne et al. 2012; Monowai) (Fig. 1B,C). For their nutrition, *V. osheai* barnacles at Brothers Seamount were shown to largely depend on the epibiotic bacteria they host, with δ^{13}C ranging from −12.0 to −12.3‰ (Suzuki et al. 2009). On the other hand, *G. gladius* and *B. manusensis* mussels are known to host gammaproteobacterial endosymbionts using the CBB cycle (Lorion et al. 2013) and exhibit ^{13}C-depleted values in vent fields from other regions (Van Audenhaege et al. 2019). Therefore, the enriched ^{13}C values of *A. niwa* may indicate a preference for food resources derived from the barnacle habitat, potentially small invertebrates, bacterial mats or detritus from the barnacles, whereas *A. dissimilis* and *A. webberi* sp. nov. from the same site might prefer organic matter derived from the mussel habitat or a mix from both habitats. The ^{15}N-enrichment of *A. niwa* from Tangaroa and Rumble V could indicate a higher trophic position for this species (Minagawa & Wada 1984), although variations in δ^{15}N are also associated with the use of different nitrogen sources with typically δ^{15}N <0‰ for ammonium and δ^{15}N values of 5–7‰ for nitrates (Lee & Childress 1994, Riekenberg et al. 2016). For instance, *R. exoculata* shrimps, which mainly feed directly on their epibiotic symbionts (Ponsard et al. 2013), exhibit unusually high δ^{15}N values for a purely chemosymbiotic species (Methou et al. 2020), which is probably related to the ability of these epibionts to use nitrates as a nitrogen source (Jan et al. 2014). Therefore, we cannot rule out that the diet of *A. niwa* is based on organic matter produced by microorganisms with a different nitrogen metabolism than food sources of *A. webberi* sp. nov. and *A. dissimilis*.

Niche theory predicts that co-occurring species always differ by their resource use and/or spatiotemporal habitat to avoid competitive exclusion when the ecosystem is at equilibrium (Hutchinson 1957, Schoener 1974). Like on the Kermadec Arc, co-occurring alvinocaridids of the Mid-Atlantic Ridge occupy distinct thermal habitats (Methou et al. 2022) and have distinct feeding habits, either purely chemosymbiotic or mixotrophic (Gebruk et al. 2000, Methou et al. 2020). In contrast, *R. variabilis* and *Nautilocaris saintlaurentae* displayed similar niches at the Fatu Kapa vent field on Futuna Arc (Methou et al. 2023a). This was attributed to the high productivity and high stochasticity of these hydrothermal vents, preventing these shrimps from exceeding the carrying capacity of their environment (Methou et al. 2023a). Thus, niche differentiation among alvinocaridids from the Kermadec Arc or the Mid-Atlantic Ridge could be linked to greater stability of these communities compared to those of the Fatu Kapa vent field.

4.3. All alvinocaridid shrimps use chemosynthetic resources across their entire depth range

Overall, alvinocaridid shrimps from the Kermadec Arc exhibited δ^{34}S < −10‰ (Fig. 5), suggesting that all individuals mainly rely on the chemosynthetic vent production (Fry et al. 1983, Reid et al. 2013) whether they inhabit sites from the upper bathyal zone such as at Rumble V (380 m depth) or deeper vent sites like Brothers Seamount (1650 m depth). This is consistent with previous work on other shallow-water vents suggesting mixed diet of photosynthetic and chemosynthetic matter at sites within the photic zone (100 m) (Comeault et al. 2010) but significant dependence on the vent endogenous produc-

tion only at sites below 200–350 m (Comeault et al. 2010, Stevens et al. 2015, Nomaki et al. 2019). An exception was found for 2 *A. dissimilis* individuals collected at the Higashi-Aogashima vent field on the Izu-Ogasawara Arc that showed $\delta^{34}S > 15‰$. These 2 individuals were characterized by small sizes and red lipid stores typical of juvenile stages of alvinocaridids (Methou et al. 2020). Ontogenetic variations from photosynthetic-derived sources to a chemosynthetic-based diet have been observed in several alvinocaridid species along their settlement phase (Stevens et al. 2008, Methou et al. 2020, 2023a) and could be responsible for the high $\delta^{34}S$ values of these 2 *A. dissimilis* juveniles.

Significant variations in the isotopic niches of alvinocaridid species could also be seen among populations from different vent fields. Niches of *A. webberi* sp. nov. and *A. dissimilis* were clearly distinct between each of their populations, with large variations in $\delta^{13}C$ and $\delta^{34}S$. Similarly, $\delta^{34}S$ values of *N. saintlaurentae* from Brothers Seamount were largely below those previously reported at Fatu Kapa (Futuna Arc) and Phoenix (North Fiji Basin) for this species (Methou et al. 2023a). To our knowledge, isotopic compositions of vent fluids were only available for Brothers Seamount (de Ronde et al. 2011), limiting comparisons between vent fields without information on their isotopic baseline composition. Nevertheless, the absence of dense mussel assemblages at Brothers Seamount (Boschen et al. 2015a) and at Higashi-Aogashima vent fields (P. Methou & C. Chen pers. obs.) could potentially explain the ^{13}C-enrichment observed for *A. webberi* sp. nov. and *A. dissimilis* at these sites. This absence of ^{13}C-depleted resources from a mussel assemblage could possibly promote a shift in the usual diet of these shrimps towards available resources within the barnacle habitat of the stalked barnacle *V. osheai* at Brothers for *A. webberi* sp. nov. and of the barnacle *Neoverruca intermedia* at Higashi-Aogashima for *A. dissimilis*. Although we cannot exclude variations of the isotopic baselines among vent fields, such a hypothesis would suggest flexible feeding habits for these 2 shrimps. Conversely, *A. niwa* showed similar niches between populations of Tangaroa and Rumble V, suggesting the same diet at both sites.

5. SYSTEMATICS

Order **Decapoda** Latreille, 1802
Family **Alvinocarididae** Christoffersen, 1986
Genus ***Alvinocaris*** Williams & Chace, 1982

5.1. *Alvinocaris dissimilis* Komai & Segonzac, 2005

(Figs. 1E, 2A–C)

Alvinocaris dissimilis Komai & Segonzac, 2005: 1158, Figs. 25, 26. — Komai & Segonzac (in: Desbruyères et al. 2006): 414, Figs. 1–4 .
Alvinocaris alexander Ahyong, 2009: 777, Figs. 1–3. — Schnabel et al. (2023): 434 (list).
Alvinocaris niwa Webber, 2004: 5–18 [part, some paratypes]. — Martin & Haney (2005): 463 [part]. — Komai & Segonzac (in: Desbruyères et al. 2006): 419 [part]. — Zelnio & Hourdez (2009): 68 (key).
Alvinocaris chelys Komai & Chan, 2010: 16, Figs. 1–6.

5.1.1. Diagnosis

Body robust. Rostrum directed downward or forward, straight, tip barely reaching first to reaching end of second antennular peduncle segment; length 0.3–0.6 × CL; dorsal margin with 9–17 teeth (6–10 teeth on rostrum proper; 3–8 postorbital); with 0–2 small ventral subdistal teeth; posterior-most tooth arising from anterior 0.17–0.31 × CL. Carapace width 0.63–0.80 × CL; dorsal angle about 145–155°. Postrostral median ridge moderately high, extending to posterior mid-length to three-quarters of carapace. Third abdominal pleuron rounded and unarmed; fourth abdominal pleuron rounded and unarmed or armed with small posteroventral tooth and additional 1–3 small teeth on posterior margin. Abdominal somite 6 length about 1.2–1.5 × height. Telson not reaching posterior margin of uropodal endopod; armed with 5–8 dorsolateral spines; posterior margin convex, with 2 pairs of posterolateral spines and 11–22 plumose setae all longer than mesial pair of lateral spines. Antennular peduncle segment 2 stout, about 1.3–1.7 times as long as wide. Distal segment of the third maxilliped setose, lacking spines along the lateral face. Pereopods 3–4 meri with 0–3 movable spines ventrolaterally; dactyli with single row of corneous spines on flexor margin, distal-most largest, proximal spines declining in size.

5.1.2. Material examined

2 females (F), ovigerous (ov.) (7.4, 9.0 mm), 1 male (M) (8.0 mm), 5 not examined, Rumble V Eastern flank, Kermadec Ridge, 36.1415–36.1420° S, 178.1997–178.2008° E, 405–408 m, Stn TAN1213/59, 26 Oct 2012, NIWA 86458.

2 F ov. (12.0, 16.0 mm), summit of Tangaroa Seamount, Kermadec Ridge, 36.3247–36.3237° S,

178.0308–178.0298° E, 667–695 m, Stn TAN1206/17, 16 Apr 2012, NIWA 89343.

1 F ov. (10.9 mm), 2 M (7.3, 9.3 mm), Clark Seamount, Kermadec Ridge, 36.452–36.4552° S, 177.8463–177.8525° E, 1030–1255 m, Stn TAN1206/39, 18 Apr 2012, NIWA 82323.

Types of *Alvinocaris alexander* material examined:

F ov. (11.9 mm), Rumble V Seamount, 36.1377–36.1327° S, 178.1957–178.195° E, 485–415, Stn TAN0107/325, 24 May 2001, NIWA 42018 (HOLOTYPE). 1 F (12.1 mm), same as holotype, NIWA 42015 (PARATYPE). 2 M (7.7, 7.8 mm), Rumble V Seamount, 36.1382–36.1445° S, 178.1957–178.1952° E, 730–470 m, Stn TAN0107/324, 24 May 2001, NIWA 42017 (PARATYPES). 2 F (11.8, 13.2 mm), Rumble V Seamount, 36.1392–36.1450° S, 178.1957–178.1930° E, 520–367 m, Stn TAN0107/233, 24 May 2001, NIWA 42016 (PARATYPES). 1 M (9.7 mm), 1 F (8.1 mm), Brothers Seamount, 34.8815–34.8812° S, 179.0627–179.0535° E, 1346–1196 m, Stn TAN0107/135, 21 May 2001, NIWA 42014 (PARATYPES).

Material for *Alvinocaris chelys* examined from Gueishandao (or Kueishan Island), Taiwan:

1 M (6.3 mm), 24.8280° N, 122.0042° E, 300–276 m, 4 Sep 2008, 2.5 m beam trawl, Stn KS 12, NTOU 00783 (PARATYPE).

2 F ov. (6.4, 7.1 mm), 1 F (6.3 mm), 2 M (CL 5.8, 5.9 mm), 24.8508° N, 121.9859° E, 253 m, 12 Aug 2010, Stn KS24, NTOU M02617.

Colour and structure:

Body pink to red colour, thin and flexible, transparent exoskeleton (Fig. 1E; NIWA 86458, male, CL = 10.5 mm).

5.1.3. Remarks

Ahyong (2009) described *A. alexander* from 2 hydrothermal vents on the Kermadec Volcanic Arc: Rumble V and Brothers Caldera. More recently, samples have been collected from similar depths (405–1255 m) on Rumble V (the type locality) and Tangaroa and Clark Seamounts further south, providing fresh specimens and the opportunity to include gene sequences into the existing phylogenetic framework (Fig. 3). COI sequences generated for *A. alexander* fall within the multi-species clade containing *A. dissimilis* Komai & Segonzac, 2005, *A. chelys* Komai & Chan, 2010 and *A. stactophila* Williams, 1988, as first shown by Yahagi et al. (2014) with several shared COI haplotypes (Fig. 4A). Within this clade, ASAP analysis on the COI gene for species delimitation failed to detect any statistically supported species-level clades, indicating that all sequences should be treated as conspecific. 18S and 28S sequences of *A. chelys* from Yang et al. (2012) and Aznar-Cormano et al. (2015), as well as *A. dissimilis* and *A. alexander* (this work) corroborate results from COI only, with a single clade for the 3 species and identical sequences for all individuals sequenced (Fig. S2). While we propose that there is sufficient evidence for the synonymy of *A. dissimilis*, *A. alexander* and *A. chelys* here, we suggest that the decision to formally dissolve *A. stactophila* requires a more detailed study.

5.1.4. Distribution

Okinawa Trough, Ryukyu Arc and Izu-Ogasawara Arc (northwestern Pacific Ocean), vents (off Gueishandao, Minami-Ensei Knoll, Higashi-Aogashima) and seeps (Kuroshima Knoll), 252–705 m. Now includes the Kermadec Volcanic Arc hydrothermal vents (Rumble V, Brothers, Tangaroa and Clark Seamounts, southwestern Pacific Ocean), 470–1346 m (most likely not distributed far below the peak of Brothers Volcano at 1197 m) (Fig. 1A).

5.2. *Alvinocaris niwa* Webber, 2004

(Figs. 1D, 2D–F)

Alvinocaris niwa Webber, 2004: 5. — Komai & Segonzac (in: Desbruyères et al. 2006): 419, Figs. 1–4 (part). — Zelnio & Hourdez (2009): 68 (key). — Webber et al. (2010): 224 (list). — Yaldwyn & Webber (2011): 188 (list). — Schnabel et al. (2023): 434 (list).

Alvinocaris sp. A. Webber & Bruce, 2002: 6 (fig., whole animal). — Batson (2003): 77 (fig. whole animal, after Webber & Bruce 2002).

5.2.1. Diagnosis

Rostrum short, not reaching to just overreaching distal margin of first segment of antennular peduncle, directed forward, weakly compressed laterally, terminating acutely, dorsal margin carinate, armed with 5–11 teeth; posterior-most tooth at about posterior orbital margin; ventral margin usually unarmed or rarely with 1 tiny subterminal tooth. Carapace somewhat compressed laterally, with sharp postros-

tral ridge reaching anterior about 0.2 of CL; antennal spine acuminate, conspicuous lobe mesial to antennal spine; pterygostomial angle weakly to somewhat produced in adults, reaching or distinctly overreaching antennal spine, terminating in sharp spine. Abdomen smooth dorsally; pleuron of third somite usually smooth, those of fourth and fifth somites at least with posterolateral tooth and frequently with additional small teeth ventrally and/or posteriorly. Telson with 5 or 7 dorsolateral spines arranged in weakly sinuous row on either side; posterior margin gently bi-lobed, with 1–3 small spines at each lateral angle and row of numerous long plumose setae, minute median spine. Eyestalks degenerated, broadly fused mesially, with small dorsomesial granule, cornea unfaceted; anterior surface unarmed; without heavily plumose bacteriophore setae. Distal segment of the third maxilliped with row of spines along the lateral face. Chela of first pereopod without fine row of long submarginal setae on outer surface along cutting edges of fingers. Second pereopod with distal movable spines on ischium; third to fifth pereopods moderately slender; dactyli armed with 2 or more rows of accessory spinules on ventral surface; meri usually unarmed; ischia of third and fourth pereopods armed usually with 2 lateral spines. Maxilliped 3 with rudimentary epipod, absent in pereopods. Appendices internae on second to fourth pereopods slender, without coupling hooks. Uropodal exopod with a single movable spine mesial to posterolateral tooth.

5.2.2. Material examined

Rumble V Seamount:

1 M (15.4 mm), 36.1413–36.1465° S, 178.1950–178.1922° E, 360–755 m, Stn TAN0107/230, 24 May 2001, HOLOTYPE (H837) NIWA 3258. 5 F (9.8, 10.0, 10.4, 11.2, 13.0 mm), 3 M (10.8, 11.0, 12.2 mm), 36.1394° S, 178.1959° E, 379 m, Stn KOK0506/16 (PV-624-3-SS-B), 30 Apr 2005, NIWA 32843. 3 M (6.1, 7.6, 8.1 mm), 2 F (5.2, 4.6 mm) NW summit, 36.1415–36.142° S, 178.1997–178.2008° E, 405–408 m, Stn TAN1213/59, 26 Oct 2012, NIWA 154064.

Tangaroa Seamount:

1 F (9.6 mm), 36.3228° S, 178.0295° E, 667 m, Stn KOK0507/32 (P5-633-7-SS3), 16 May 2005, NIWA 70346. 1 F (12.8 mm), 4 M (8.2, 9.0, 12.8, 14.0 mm), 36.3233° S 178.0303° E, 653 m, Stn KOK0507/12 (PV-629-19SS), 12 May 2005, NIWA 32842. 13 M (10.0–15.3 mm), 4 F ov. (13.5–14.3 mm), 2 F (12.0, 14.0 mm), 20 specimens (not examined), summit, 36.3247–36.3237° S, 178.0308–178.0298° E, 667–695 m, Stn TAN1206/17, 16 Apr 2012, NIWA 82117.

Colour and structure:

Pink to red, blind, with a thin and flexible exoskeleton (Fig. 1D, live colouration of an undetermined specimen from TAN1206/17, NIWA 82117).

5.2.3. Remarks

Specimens presented here for *A. niwa* conform well with Webber's (2004) detailed description of the holotype. The length of the postorbital carapace ranges from 7.4–15.0 mm for females (ovigerous from 13.5 mm), 6.1–15.3 mm for males and 4.6–5.2 mm for 2 juveniles (NIWA 154064). Total body length is 17–54 mm, and the number of rostral spines is 5–11 (median = 8); the rostrum did not reach the end of the first antennular segment in more than half of the specimens, while about a third had a rostrum that slightly over-reached it. The second antennular segment length:width ratio ranges from 1.1 to 2.0, with juveniles having the stoutest segments and only slightly positive relationship towards more slender segments for larger adults. The telson length:width ratio is 2.5–1.9, with a slight trend towards a stouter telson in the larger adults. Sexual dimorphism in the size of the first pereopod palm is distinct, with the larger males (CL $\geqslant$ 14 mm) having both an inflated palm relative to the fingers (palm length vs. finger length $\geqslant$0.8) and an elongated palm (length:width ratio >1) compared to females or smaller males.

5.2.4. Distribution

Endemic to active hydrothermal vents on southern Kermadec Volcanic Arc; Brothers, Rumble V and Tangaroa Seamounts, 379–1538 m (most likely not distributed far below the peak of Brothers Volcano at 1197 m) (Fig. 1A).

5.3. *Alvinocaris webberi* sp. nov. Schnabel & Methou

(Figs. 1F, 6, 7)

ZooBank registration LSID: urn:lsid:zoobank.org:act:190DB608-594A-4264-B0A7-6569432C5DB3

Alvinocaris longirostris Webber, 2004: 5, Figs. 5, 6a–f (whole female, diagnostic characters). — Ahyong (2009): 776. — Webber et al. (2010): 224 (list). —

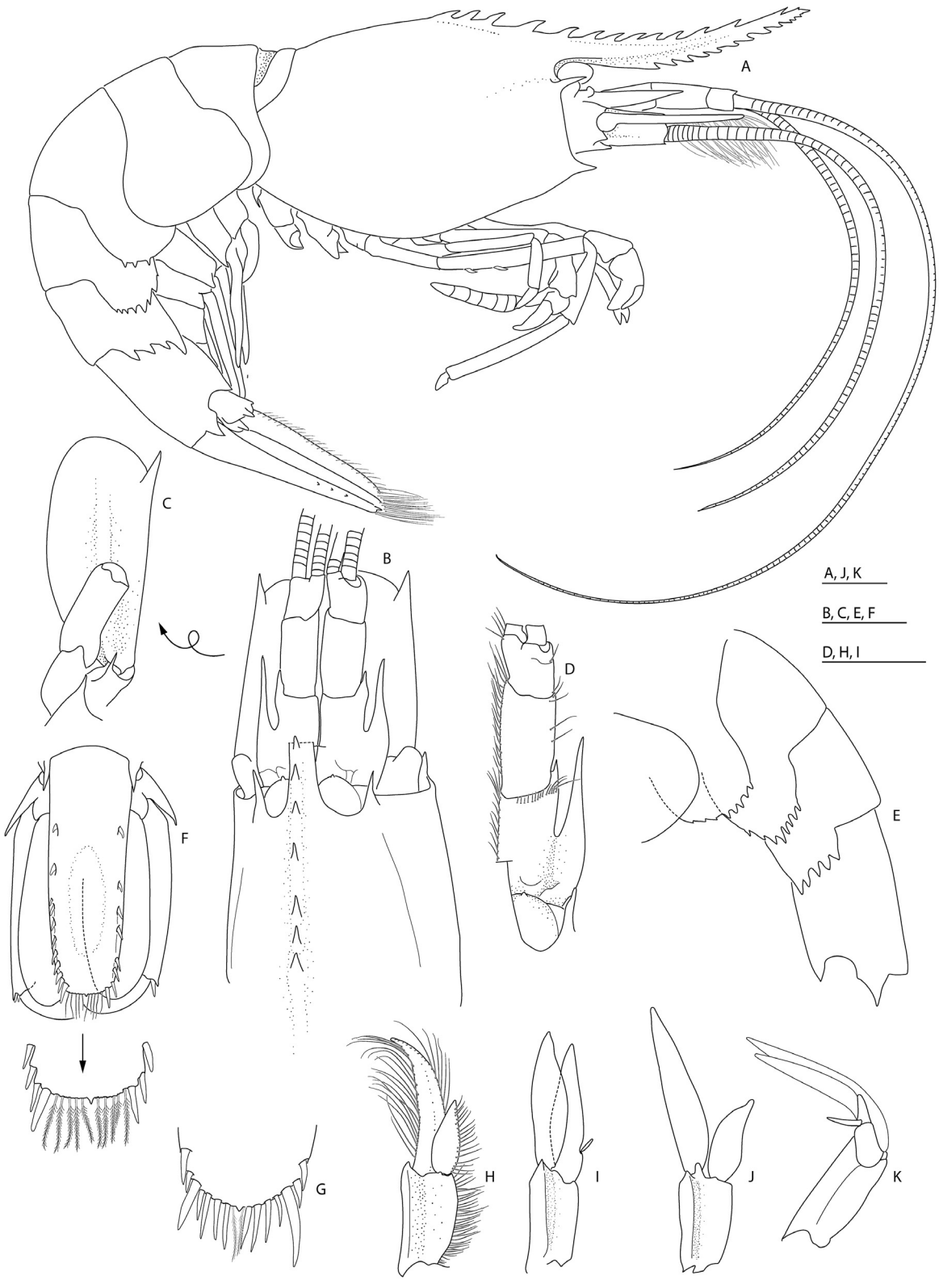

Fig. 6. *Alvinocaris webberi* sp. nov. (A–F, H ,I) Holotype female, NIWA 64616; (G) juvenile, NIWA 162651, carapace length (CL) 6.6 mm; (J,K) male, NIWA 32846, CL 11.0 mm. (A) Habitus, right, lateral. (B) Anterior cephalothorax, dorsal. (C) Antennal scale, ventral. (D) Antennule, dorsal. (E) Abdominal segments 2–6, left, lateral. (F) Telson and uropods, dorsal (closeup of posterior margin of telson). (G) Posterior margin of telson, dorsal. (H, J) First pleopod, ventral. (I, K) Second pleopod, ventral. Scale bars = 2 mm

Fig. 7. *Alvinocaris webberi* sp. nov. (A–F) female paratype, NIWA 64625, carapace length (CL) 6.5 mm; (G–L) holotype female, NIWA 64616. (A) Mandible, left, convex view. (B) Maxillule, left, ventral. (C) Maxilla, ventral. (D) First maxilliped, ventral, inset view of endopod of first maxilliped, dorsal. (E) Second maxilliped, ventral; inset: view of epipod and podobranch, dorsal. (F) Third maxilliped, ventral. (G) Right pereopod 1 merus and chela, mesial. (H) Left pereopod 1, lateral. (I) Left pereopod 2, lateral. (J) Right pereopod 3, with detail of distal propodus and dactylus. (K) Right pereopod 4. (L) Left pereopod 5. Scale bars: 1 mm (A), 2 mm (B–L)

Yaldwyn & Webber (2011): 188 (list). — Schnabel et al. (2023): 434 (list).

A. cf. *lusca* Wright et al. (1998): 342.

Alvinocaris sp. B Webber & Bruce, 2002: 6 (fig. whole animal).

5.3.1. Diagnosis

Rostrum directed forward, straight or weakly curved dorsally, 0.4–1.2 × CL, usually overreaching distal margin of second or third antennular segment, armed with 9–16 teeth including 3–7 relatively large teeth on carapace posterior to orbital margin, posteriormost tooth arising at about anterior third of CL; ventral margin armed with 2–14 (usually 7–9) small teeth on anterior 0.3–0.7. Carapace width 0.56–0.70 × CL; postrostral median ridge relatively high, dorsal angle about 155–170°; branchial region not notably inflated, slightly convex; pterygostomial tooth strong. Third abdominal pleura usually with 3–5 posterolateral denticles. Fourth abdominal pleura with 5–10 teeth around posteroventral corner. Fifth abdominal pleura armed with 3–5 strong posteroventral teeth. Telson not reaching to reaching posterior margin of uropodal endopod, length 4.5–6.9 longer than posterior width, posterior width about half of anterior width, usually armed with 7 or 8 dorsolateral spines; posterior margin shallowly convex, with small median spine and 2 pairs of spines at lateral angles, furnished with 7 to 14 plumose setae along margin. Eye with small spiniform tubercle on anterior surface. Antennular peduncle with second segment 1.5–2.1 times longer than wide. Antennal scale about half length of carapace, around twice as long as wide. Third maxilliped dactylus without spines. Distal segment of the third maxilliped setose, lacking spines along the lateral face. Third to fifth pereopods moderately slender; dactyli each with single row of accessory spinules; meri armed usually with 3 spines on ventrolateral surfaces, meri of fifth pereopod usually unarmed but may have 1 or 2 spines; ischia with 1 or 2 spines on third and fourth pereopods, unarmed on fifth pereopod. Second to fourth pleopods each with slender appendix interna. Appears both at hydrothermal vents and seeps.

5.3.2. Etymology

Named after W. Richard Webber, former Curator of Crustacea at the Museum of New Zealand Te Papa Tongarewa, who described the first species of *Alvinocaris* from Aotearoa/New Zealand.

5.3.3. Material examined

HOLOTYPE

F (CL 17.1 mm), Brothers Seamount 34.8825–34.8822° S, 179.068–179.0717° E, 1201–1360 m, Stn TAN1007/92, 05 Jun 2010, NIWA 64616.

PARATYPES

1 F (12.1 mm), Brothers Seamount, 34.8782° S, 179.0558–179.0822° E, 1538–1197 m, Stn TAN0107/141, 22 May 2001, NIWA 3262. 1 F (6.5 mm), 34.8822–34.8822° S, 179.0662–179.0702° E, 1199–1221 m, Stn TAN1007/94, 05 Jun 2010, NIWA 64625.

1 F ov. (10.1 mm), 7 F (9.5–13.2 mm), 4 M (9.0, 9.0, 10.0, 11.4 mm), Tangaroa Seamount, summit, 36.3247–36.3237° S, 178.0308–178.0298° E, 667–695 m, Stn TAN1206/17, 16 Apr 2012, NIWA 88913.

Additional material:

Monowai Seamount, active vent:

1 M (11.0 mm), 25.8072° S, 177.16817° W, 1064 m, Stn KOK0505/7, 25.8072° S, 177.1682° W, 08 Apr 2005, NIWA 32846. 2 juveniles (5.2, 7.5 mm), 25.8042° S, 177.1685° W, 1143 m, Stn KOK0505/14, 10 Apr 2005, NIWA 32850. 1 F ov. (11.8 mm), 2 F (13.5, 15.0 mm), 1 M (11.8 mm) 17, SW caldera wall, 25.8048–25.8098° S, 177.1698–177.1637° W, 1140–1054 m, Stn TAN0411/6, 03 Oct 2004, NIWA 115094.

Havre Volcano:

1 F ov. (13.3 mm), southern caldera and rim, 31.1263° S, 179.0394° W, 881.9 m, RV 'Roger Revelle' (RR1506) Stn J2-802/HVR0033, 30 Mar 2015, NIWA 126541.

Brothers Seamount, active vent:

3 damaged specimens (8.5–11.0 mm), 34.8787° S, 179.0717° E, 1336 m, RV 'Yokosuka' DSV 'Shinkai 6500' Dive #854, 01 Nov 2004, NIWA 4080. 1 F ov. (11.2 mm), 3 F (8.0–9.6 mm), Satellite Cone, 34.8779–34.8798° S, 179.0721–179.0705° W, 1316–1362 m, RV 'Thomas Thompson' Stn TN230/D09A-01, 07 Mar 2009, NIWA 48479.

Tangaroa Seamount, active vent:

2 F ov. (9.5, 9.8 mm), 1 M (9.7 mm), 36.3228° S, 178.0295° E, 667 m, Stn KOK0507/32, 16 May 2005, NIWA 32848.

Southern Hikurangi Margin, hydrocarbon seep:

1 M (14.5 mm), Glendhu Ridge seep, 41.7657° S, 176.0825° E, 1980–2000 m, epibenthic sled, Stn TAN1904/50, 11 Jul 2019, NIWA 140415. 1 M (6.4 mm), 41.7863° S, 176.2098° E, 2300 m, ROV

'ROPOS', 8 Mar 2021, Stn TAN2102_R2137, NIWA 162645. 1 F ov. (10.0 mm), 41.7863° S, 176.2098° E, 2300 m, ROV 'ROPOS', 8 Mar 2021, Stn TAN2102_R2137, NIWA 162646. 1 F (11.5 mm), 41.7863° S, 176.2098° E, 2300 m, ROV 'ROPOS', 8 Mar 2021, Stn TAN2102_R2137, NIWA 162647. 1 M (7.7 mm), 41.7863° S, 176.2098° E, 2300 m, ROV 'ROPOS', 8 Mar 2021, Stn TAN2102_R2137, NIWA 162648. 1 juv. (4.4 mm), 41.7863° S, 176.2098° E, 2300 m, ROV 'ROPOS', 8 Mar 2021, Stn TAN2102_R2137, NIWA 162649.

1 F ov. (11.3 mm), 2 M (9.0, 10.5 mm), 41.76833° S, 176.0885° E, 1986 m, ROV 'ROPOS', 9 Mar 2021, Stn TAN2102_R2138, NIWA 162650. 2 juv. (6.6, 6.6 mm), 41.76833° S, 176.0885° E, 1986 m, ROV 'ROPOS', 9 Mar 2021, Stn TAN2102_R2138, NIWA 162651.

Specimens presented by Webber (2004) from Brothers Seamount caldera (NIWA 3262–3276, 341 specimens, NMNZ CR.9978–9988, 33 specimens).

5.3.4. Description

[Numbers in square brackets are measurements for the holotype]

Body glabrous. Rostrum directed forward, straight to curved distally, about 0.6–1.5 [0.9] times as long as carapace, falling short or overreaching distal end of antennular peduncle; dorsal margin armed with 9–16 [14] teeth, including 6–11 [9] teeth on rostrum proper and 3–7 [5] postorbital, posterior-most tooth arising at about [0.6]–0.7 length of carapace; ventral margin armed with 2–14 [12] teeth; lateral carina distinct along full length, merging into orbital margin. Carapace 0.65– [0.68] times as wide as long; dorsal angle 155– [160]°; with postrostral carina extending past mid-length, [0.6] 0.8 CL; antennal tooth pronounced, directed slightly dorsally; pterygostomial tooth strong, acuminate, distinctly overreaching tip of antennal tooth; post-antennal groove shallow; anterior part of branchial region not inflated.

Abdomen with third pleura marginally with up to 11 [7] small denticles but may be unarmed. Fourth pleura with 3–10 spines, sub-acute posteroventral tooth present, with additional denticles along posterior and ventral margins. Fifth pleura rarely unarmed, usually with 2–6 [4/5] teeth on posterior margin, ventral margin may be serrated or smooth. Sixth pleuron [1.6]–1.7 times longer than proximal height, with strong, acute posteroventral tooth. Telson barely reaching to falling short of posterior margin of uropodal endopod, about [3.0]–3.2 times longer than anterior width and about [5]–8 times longer than posterior width, armed with 7–11 dorsolateral spines on either side, including paired spines on distolateral corners, distal-most spine longest, straight; posterior margin convex to slightly notched, usually projected into small triangular tooth medially, with 7–14 [10] plumose setae (numbers on either side of median typically uneven). Eye anterior surface bearing one small, spinelike tubercle.

Antennular peduncle reaching distal margin of antennal scale. First segment with strong distolateral tooth, reaching about 1/3 length of second segment of antennular peduncle; stylocerite slender, reaching about mid-length of second segment of antennular peduncle. Second peduncular segment 1.5–2.1 [1.76] times as long as wide, with distomesial spine. Antennal scale 2.1– [2.2] times longer than wide, lateral margin nearly straight; distolateral tooth directed straight forward; dorsal carina distinct, slightly diverging from lateral margin; distal lamella rounded.

Mandible with incisor process bearing about 6 unequal teeth on distal margin; molar process slender, tip rounded, without setae; palp bi-articulated. Maxillule with dense setae on inner margin of both distal and basal endite; palp slightly bilobed, distomesial lobe with 1 apical plumose seta, distolateral lobe rounded, without seta. Maxilla with scaphognathite moderately broad; palp slender, tapering; distal endite deeply bilobed; proximal endite with single lobe. First maxilliped with large leaf-like exopod, anterior margin smooth; basal endite about half length of exopod; epipod simple. Second maxilliped with relatively stout endopod; epipod sub-ovate, bearing slender podobranch, distally gently or distinctly bi-lobed. Third maxilliped ultimate segment distinctly longer than penultimate segment, trigonal in cross section, tapering, bearing 2 spines distally; lateral surface unarmed; mesial surface flat, with rows of dense setae; epipod widened distally, subtriangular. First pereopod moderately slender, symmetrical in size and shape; chela sexually dimorphic with palms most distinctly inflated in large males; fingers curved downward and inward, cutting edges each armed with comb-like row of uniform setae; carpus distal half of flexor margin flared into prominent ridge ending in strong tooth, ventrodistal tooth absent; mesial surface ventrally with grooming apparatus consisting of patch of short stiff setae, with proximal tooth present; merus and ischium unarmed. Second pereopod shorter and more slender than first; chela slightly shorter than carpus; fingers slightly longer than palm, curved distally and crossing each other when closed; ischium armed with 1 (rarely no) spine ventrolaterally. Third and fourth pereopods slender; dactylus 0.14 times as long as propodus, ter-

minating in strong, clearly demarcated unguis, bearing single row of 5–6 accessory moveable spines on flexor margin over almost entire length; propodus with slender spinules on ventral surface; carpus distinctly shorter than propodus, unarmed; merus slightly longer than propodus, armed with 3 (rarely 2) moveable spines on lateral surface ventrally; ischium armed with 2 (rarely 1) moveable spines on lateral surface ventrally. Fifth pereopod generally similar to third and fourth pereopods, propodus with numerous spiniform setulose setae on ventral surface, arranged in longitudinal rows; merus with [1] or 2 spines or unarmed; ischium usually unarmed. Pleopods typically sexually dimorphic; endopod of first pleopod about half length of exopod, distal part of male feebly bilobed, simple in females. Endopod of second pleopod with appendix interna only in females; appendix masculina in males, slightly shorter than appendix interna. Uropodal rami both reaching or slightly overreaching posterior margin of telson; exopod slightly longer than endopod, with 1 or 2 small movable spines just mesial to smaller posterolateral tooth.

Size: CL 4.4–15.0 mm, ovigerous from 9.5 mm, TL to approximately 53 mm.

Colour and structure: Body with thin and transparent exoskeleton with diffuse red reticulation on carapace and anterior half of abdomen, eyes unpigmented (Fig. 1F, live colouration of holotype female, NIWA 64616).

5.3.5. Remarks

Webber (2004) provided a detailed description of about 400 specimens collected from 7 stations around the Brothers Caldera during 2 surveys (1996 and 2001) that he assigned to *A. longirostris.* Considering clear indications of genetic isolation provided in this study, those specimens are assigned to a new species, *Alvinocaris webberi* sp. nov. Additional material is provided for 3 further vent sites on the Kermadec Volcanic Arc and 2 carbon seeps on the Hikurangi Margin, the southern extension of the Tonga-Kermadec subduction system (Turco et al. 2022).

A. webberi sp. nov. is aligned with those congeners that have a long rostrum, typically at least reaching the end of the antennular peduncle, bearing dorsal teeth that extend from the rostrum to a portion of the carapace posterior to the orbital margin, and bearing at least 3 ventral rostral spines, the carapace without strongly inflated branchial region or deep post-antennal groove, and the posterior margin of the telson nearly always with 2 pairs of lateral spines and a number of plumose setae along the margin (but see comments on variation below). This includes *A. longirostris, A. markensis* Williams, 1988 and *A. muricola* Williams, 1988. The former was described from vents around the Okinawa Trough and subsequently found on seeps off Japan, first reported by Fujikura (1995). The latter are known from vents (*A. markensis*) and seeps (*A. muricola*) in the Atlantic Ocean and the Gulf of Mexico; however, Teixeira et al. (2013) questioned the validity of these 2 species based on genetic analysis from across their range. A formal taxonomic revision of these species is pending.

Finding fixed apomorphies for species of *Alvinocaris* appears to be difficult, with high levels of intraspecific morphological variation being frequently noted. We followed the assessment of Komai & Segonzac (2005) with regards to characters useful to discriminate species. *A. webberi* sp. nov. overlaps in most characters with the aforementioned congeners, including specimen size range, length of rostrum compared to CL and spination. It appears that the posterior-most rostral tooth is situated slightly more posterior compared to the other species (0.36–0.67 × CL, compared to 0.24–0.48 × CL for the other species). The armature of abdominal pleura 4 varies slightly, armed with 5–10 teeth in *A. webberi* sp. nov., with 1–4 teeth in the other species. The telson varies, with *A. webberi* sp. nov. having a small median spine situated on the convex posterior margin of the telson, absent in the other species; and the shape of the telson varies slightly, with the ratio between the telson length and the posterior width ranging from 4.5–6.9 in adults (up to 8.4 in the smallest juvenile), although this overlaps with ranges reported for *A. longirostris* (4.10–4.90) and *A. muricola/A. markensis* (4.90–5.20). Other typically useful characters such as the shape and size of the antennular and antennal peduncles or the spination of pereopods 3–5 are sufficiently variable to overlap with all other species. While not generally used for species discrimination, we note differences that might warrant further examination as to their utility: the second maxilliped bears a sub-ovate epipod that reaches to about half the length of the ischium and a weakly or distinctly bilobed podobranch; the shape and size differs from those illustrated for the other species. The shape of the epipod on the third maxilliped is subtriangular in *A. webberi* sp. nov., similar to that illustrated for *A. muricola* by Komai & Segonzac (2005), but different from the finger-like projection illustrated for *A. longirostris* by Kikuchi & Ohta (1995).

In the absence of constant characters for specimens found thus far at 2 sites in methane seeps along the

Hikurangi Margin and considering the genetic similarity between populations from the Kermadec volcanoes and the Hikurangi seeps, the populations are considered conspecific. A notable variation is observed in 2 of the 11 specimens examined from seep sites: the posterior margin of the telson is in both cases furnished with 8 spines instead of plumose setae as observed for all other specimens (Fig. 6), with only 2 longer plumose setae adjacent to the median spine. These specimens otherwise align morphologically and genetically with the other specimens assigned to *A. webberi* sp. nov. (see Aw46, Fig. 3).

5.3.6. Distribution

Endemic, Kermadec Volcanic Arc, hydrothermal vents of Monowai, Havre, Brothers, Rumble V and Tangaroa Seamounts, cold seep 'Glendhu Ridge' on the southern Hikurangi Margin, 667–2000 m (Fig. 1A).

Order **Decapoda** Latreille, 1802
Family **Alvinocarididae** Christoffersen, 1986
Genus ***Nautilocaris*** Komai & Segonzac, 2004

5.4. *Nautilocaris saintlaurentae* Komai & Segonzac, 2004

Nautilocaris saintlaurentae Komai & Segonzac, 2004: 1180, Figs. 2–6 [type locality: North Fiji Basin, White Lady Site, 2000 m]. — Ahyong (2009): 785, Fig. 4. — Vereshchaka et al. (2015): 4, 19, Figs. 4–6. — Schnabel et al. (2023): 434 (list).

5.4.1. Diagnosis

Rostrum carinate and dentate dorsally, reaching distal margin of basal segment of antennular peduncle; ventral surface unarmed. Carapace somewhat compressed laterally; postrostral median carina low, blunt, restricted to anterior 0.15 of carapace; antennal tooth acuminate; pterygostomial angle weakly produced anteriorly, extending as far as antennal spine, terminating in sharp tooth. Third to fifth pleonal pleura dentate posteroventrally. Telson with 7–9 dorsolateral spines arranged in slightly sinuous row; posterior margin convex, bearing 12–19 spines in total, 1–3 spines at each posterolateral corner shorter than mesial spines, simple, while remaining mesial spines are elongate, bearing minute marginal setules. Eyes rather large but degenerate, broadly fused mesially; anterior surface smooth; no trace of pigment. Antennal scale broadly oval, with distinct dorsolateral tooth. Chela of first pereopod with fine row of long submarginal setae on outer surface along cutting edges of fingers. Third to fifth pereopods moderately slender to stout; each dactylus armed with single row of accessory spinules on ventral margin; meri unarmed; ischia with spines in third, usually unarmed in fourth and fifth. Third maxilliped to fourth pereopods with strap-like, terminally hooked epipods, corresponding to setobranchs above first to fifth pereopods; appendices internae on second to fourth pereopods rudimentary. (After Komai & Segonzac 2004.)

5.4.2. Distribution

Known from hydrothermal vents on the North Fiji Basin, Lau Basin, Tonga Arc, Kulo Lasi on the Futuna Arc and Brothers Caldera on the Kermadec Arc, at depths of 1604–2000 m (Komai & Segonzac 2004, Ahyong 2009, Vereshchaka et al. 2015, Komai et al. 2016).

Data availability. Sequences have been deposited in GenBank under accession numbers OR750757–OR750768 for 28S, OR750745–OR750756 for 18S and OR734008–OR734016 and OR766468–OR766495 for COI (see Table S1 for sampling summary with associated individual ID). Metadata associated with each shrimp, including research vessel and research expedition ID, collection date, sampling location, storage conditions, life stage and body size, are displayed in Table S1. Isotopic ratios of each individual are also available in Table S1.

Acknowledgements. We thank the NIWA Invertebrate Collection team and Dr. Belinda Alvarez de Glasby of the NMNZ Natural History team for their tireless efforts. We also thank Dr. Tin-Yam Chan from NTOU for a loan of *A. chelys* specimens. We thank the captains and crews of the different research cruises of the RV 'Tangaroa' (TAN0107, TAN0411, TAN1007, TAN1206, TAN1213, TAN1904, TAN2102), RV 'Ka'imikai-o-Kanaloa' (KOK0505, KOK0506, KOK0507), RV 'Yokosuka' (YK04-09, YK22-05), RV 'Shinsei-Maru' (KS-21-20) and RV 'Roger Revelle' (RR1506). We also thank the pilots and the operation team of the HOVs 'Shinkai 6500' and 'Pisces V' as well as of the ROVs 'Hyper-Dolphin' and 'ROPOS' during these research cruises. We gratefully acknowledge the chief scientists of the relevant expeditions: Gary Massoth and Bob Embley (NOAA; KOK0505, KOK0506, KOK0507), Tatsuo Nozaki (JAMSTEC; KS-21-20), Ken Takai (JAMSTEC; YK04-09, YK22-05), Malcolm Clark (NIWA; TAN1007, TAN1206), Richard Wysoczanski (NIWA; TAN1213), Ashley Rowden (NIWA; TAN1904), Adam Soule (Woods Hole Oceanographic Institution) and Rebecca Carey (University of Tasmania) (RR1506), and Laura Wallace (New

Zealand Institute of Geological and Nuclear Sciences; TAN2102). P.M. was supported by a JAMSTEC Young Research Fellow fellowship. C.C., N.O.O., N.O. and H.N. were supported by Grants-in-Aid for Scientific Research (KAKENHI) from the Japan Society for the Promotion of Science (JSPS), grant codes 18K06401, 21H012037, 20H00208 and 23H02541, respectively. K.E.S. was funded by NIWA under Coasts and Oceans Research Programme 2 Marine Biological Resources: discovery and definition of the marine biota of New Zealand (2022–2023). Sample collections were conducted with funding from the following agencies: New Zealand Ministry for Business, Innovation and Employment (former New Zealand Foundation for Research, Science and Technology), the Ministry for Primary Industries, Auckland University, University of Tasmania, New Zealand Institute of Geological and Nuclear Sciences (GNS), Woods Hole Oceanographic Institute, the United States National Science Foundation and NIWA. Faunal collections were conducted in New Zealand or the Japanese exclusive economic zone by New Zealand or Japanese government research vessels. Research animals were invertebrates (caridean shrimps), with no live experiments caried out on animals for this study.

LITERATURE CITED

Adams DK, Arellano SM, Govenar B (2012) Larval dispersal: vent life in the water column. Oceanography 25:256–268

Ahyong ST (2009) New species and new records of hydrothermal vent shrimps from New Zealand (Caridea: Alvinocarididae, Hippolytidae). Crustaceana 82:775–794

Aznar-Cormano L, Brisset J, Chan TY, Corbari L and others (2015) An improved taxonomic sampling is a necessary but not sufficient condition for resolving inter-families relationships in Caridean decapods. Genetica 143:195–205

Baco AR, Rowden AA, Levin LA, Smith CR, Bowden DA (2010) Initial characterization of cold seep faunal communities on the New Zealand Hikurangi margin. Mar Geol 272:251–259

Bandelt HJ, Forster P, Röhl A (1999) Median-joining networks for inferring intraspecific phylogenies. Mol Biol Evol 16:37–48

Batson P (2003) Deep New Zealand — blue water, black abyss. Canterbury University Press, Christchurch

Borda E, Kudenov JD, Chevaldonné P, Blake JA and others (2013) Cryptic species of *Archinome* (Annelida: Amphinomida) from vents and seeps. Proc R Soc B 280:20131876

Boschen RE, Rowden AA, Clark MR, Barton SJ, Pallentin A, Gardner JPA (2015a) Megabenthic assemblage structure on three New Zealand seamounts: implications for seafloor massive sulfide mining. Mar Ecol Prog Ser 523:1–14

Boschen RE, Rowden AA, Clark MR, Gardner JPA (2015b) Limitations in the use of archived vent mussel samples to assess genetic connectivity among seafloor massive sulfide deposits: a case study with implications for environmental management. Front Mar Sci 2:105

Bowden DA, Rowden AA, Thurber AR, Baco AR, Levin LA, Smith CR (2013) Cold seep epifaunal communities on the Hikurangi Margin, New Zealand: composition, succession, and vulnerability to human activities. PLOS ONE 8: e76869

Buckeridge JS (2000) *Neolepas osheai* sp. nov., a new deep-sea vent barnacle (Cirripedia: Pedunculata) from the Brothers Caldera, south-west Pacific Ocean. NZ J Mar Freshw Res 34:409–418

Comeault A, Stevens CJ, Juniper SK (2010) Mixed photosynthetic-chemosynthetic diets in vent obligate macroinvertebrates at shallow hydrothermal vents on Volcano 1, South Tonga Arc — evidence from stable isotope and fatty acid analyses. Cah Biol Mar 51:351–359

de Ronde CEJ, Massoth GJ, Butterfield DA, Christenson BW and others (2011) Submarine hydrothermal activity and gold-rich mineralization at Brothers Volcano, Kermadec Arc, New Zealand. Miner Depos 46:541–584

Desbruyères D, Segonzac M, Bright M (2006) Handbook of deep-sea hydrothermal vent fauna, 2nd edn. Biologiezentrum der Oberösterreichischen Landesmuseen, Linz

Excoffier L, Smouse PE, Quattro JM (1992) Analysis of molecular variance inferred from metric distances among DNA haplotypes: application to human mitochondrial DNA restriction data. Genetics 131:479–491

Flaherty EA, Ben-David M (2010) Overlap and partitioning of the ecological and isotopic niches. Oikos 119:1409–1416

Fry B, Gest H, Hayes JM (1983) Sulphur isotopic compositions of deep-sea hydrothermal vent animals. Nature 306: 51–52

Fu YX, Li WH (1993) Statistical tests of neutrality of mutations. Genetics 133:693–709

Fujikura K, Hashimoto J, Fujiwara Y, Okutani T (1995) Community ecology of the chemosynthetic community at Off Hatsushima site, Sagami Bay, Japan. JAMSTEC J Deep Sea Res 11:227–241 (in Japanese with English summary)

Gebruk AV, Southward EC, Kennedy H, Southward AJ (2000) Food sources, behaviour, and distribution of hydrothermal vent shrimps at the Mid-Atlantic Ridge. J Mar Biol Assoc UK 80:485–499

He X, Xu T, Chen C, Liu X and others (2023) Same (sea) bed different dreams: Biological community structure of the Haima seep reveals distinct biogeographic affinities. Innov Geosci 1:100019

Hernández-Ávila I, Cambon-Bonavita MA, Pradillon F (2015) Morphology of first zoeal stage of four genera of alvinocaridid shrimps from hydrothermal vents and cold seeps: implications for ecology, larval biology and phylogeny. PLOS ONE 10:e0144657

Huelsenbeck JP, Ronquist F (2001) MRBAYES: Bayesian inference of phylogenetic trees. Bioinformatics 17:754–755

Hügler M, Sievert SM (2011) Beyond the Calvin Cycle: autotrophic carbon fixation in the ocean. Annu Rev Mar Sci 3: 261–289

Hutchinson GE (1957) Concluding remarks. Cold Spring Harbor Symp Quant Biol 22:415–427

Iizasa K, Asada A, Mizuno K, Katase F, Lee S, Kojima M, Ogawa N (2019) Native gold and gold-rich sulfide deposits in a submarine basaltic caldera, Higashi-Aogashima hydrothermal field, Izu-Ogasawara frontal arc, Japan. Miner Depos 54:117–132

Isaji Y, Ogawa NO, Takano Y, Ohkouchi N (2020) Quantification and carbon and nitrogen isotopic measurements of heme B in environmental samples. Anal Chem 92: 11213–11222

Jackson AL, Inger R, Parnell AC, Bearhop S (2011) Comparing isotopic niche widths among and within communities: SIBER — Stable Isotope Bayesian Ellipses in R. J Anim Ecol 80:595–602

Jan C, Petersen JM, Werner J, Teeling H and others (2014) The gill chamber epibiosis of deep-sea shrimp *Rimicaris exoculata*: an in-depth metagenomic investigation and discovery of *Zetaproteobacteria*. Environ Microbiol 16: 2723–2738

Kikuchi T, Ohta S (1995) Two caridean shrimps of the families Bresiliidae and Hippolytidae from a hydrothermal field on the Iheya Ridge off the Ryuku Islands, Japan. J Crustac Biol 15:771–785

Komai T, Chan TY (2010) A new genus and two new species of alvinocaridid shrimps (Crustacea: Decapoda: Caridea) from a hydrothermal vent field off northeastern Taiwan. Zootaxa 2372:15–32

Komai T, Segonzac M (2004) A new genus and species of alvinocaridid shrimp (Crustacea: Decapoda: Caridea) from hydrothermal vents on the North Fiji and Lau Basins, south-western Pacific. J Mar Biol Assoc UK 84: 1179–1188

Komai T, Segonzac M (2005) A revision of the genus *Alvinocaris* Williams and Chace (Crustacea: Decapoda: Caridea: Alvinocarididae), with descriptions of a new genus and a new species of *Alvinocaris*. J Nat Hist 39: 1111–1175

Komai T, Tsuchida S (2015) New records of Alvinocarididae (Crustacea: Decapoda: Caridea) from the southwestern Pacific hydrothermal vents, with descriptions of one new genus and three new species. J Nat Hist 49: 1789–1824

Komai T, Menot L, Segonzac M (2016) New records of caridean shrimp (Crustacea: Decapoda) from hydrothermally influenced fields off Futuna Island, Southwest Pacific, with description of a new species assigned to the genus *Alvinocaridinides* Komai & Chan, 2010. Zootaxa 4098: 298–310

Lee RW, Childress JJ (1994) Assimilation of inorganic nitrogen by marine invertebrates and their chemoautotrophic and methanotrophic symbionts. Appl Environ Microbiol 60:1852–1858

Leigh JW, Bryant D (2015) POPART: full-feature software for haplotype network construction. Methods Ecol Evol 6: 1110–1116

Levin LA, Baco AR, Bowden DA, Colaco A and others (2016) Hydrothermal vents and methane seeps: rethinking the sphere of influence. Front Mar Sci 3:72

Leybourne MI, Schwarz-Schampera U, de Ronde CEJ, Baker ET and others (2012) Submarine magmatic-hydrothermal systems at the Monowai volcanic center, Kermadec Arc. Econ Geol 107:1669–1694

Lorion J, Kiel S, Faure B, Kawato M and others (2013) Adaptive radiation of chemosymbiotic deep-sea mussels. Proc R Soc B 280:20131243

Martin JW, Haney TA (2005) Decapod crustaceans from hydrothermal vents and cold seeps: a review through 2005. Zool J Linn Soc 145:445–522

McCowin MF, Rowden AA, Rouse GW (2019) A new record of *Lamellibrachia columna* (Siboglinidae, Annelida) from cold seeps off New Zealand, and an assessment of its presence in the western Pacific Ocean. Mar Biodivers Rec 12:10

McCowin MF, Collins PC, Rouse GW (2023) Updated phylogeny of Vestimentifera (Siboglinidae, Polychaeta, Annelida) based on mitochondrial genomes, with a new species. Mol Phylogenet Evol 187:107872

McCutchan JH, Lewis WM, Kendall C, McGrath CC (2003) Variation in trophic shift for stable isotope ratios of carbon, nitrogen, and sulfur. Oikos 102:378–390

Methou P, Michel LN, Segonzac M, Cambon-Bonavita MA, Pradillon F (2020) Integrative taxonomy revisits the ontogeny and trophic niches of *Rimicaris* vent shrimps. R Soc Open Sci 7:200837

Methou P, Hernández-Ávila I, Cathalot C, Cambon-Bonavita MA, Pradillon F (2022) Population structure and environmental niches of *Rimicaris* shrimps from the Mid-Atlantic Ridge. Mar Ecol Prog Ser 684:1–20

Methou P, Cueff-Gauchard V, Michel LN, Gayet N, Pradillon F, Cambon-Bonavita M (2023a) Symbioses of alvinocaridid shrimps from the South West Pacific: no chemosymbiotic diets but conserved gut microbiomes. Environ Microbiol Rep 15:614–630

Methou P, Nye V, Copley JT, Watanabe HK, Nagai Y, Chong C (2023b) Life-history traits of alvinocaridid shrimps inhabiting chemosynthetic ecosystems around Japan. Mar Biol 170:75

Methou P, Chen C, Komai T (2024) Revision of the alvinocaridid shrimp genus *Rimicaris* Williams & Rona, 1986 (Decapoda: Caridea) with description of a new species from the Mariana Arc hydrothermal vents. Zootaxa 5406: 501–518

Minagawa M, Wada E (1984) Stepwise enrichment of ^{15}N along food chains: further evidence and the relation between $\delta^{15}N$ and animal age. Geochim Cosmochim Acta 48:1135–1140

Miura T, Kojima S (2006) Two new species of vestimentiferan tubeworm (Polychaeta: Siboglinidae a.k.a. Pogonophora) from the Brothers Caldera, Kermadec Arc, South Pacific Ocean. Species Divers 11:209–224

Moalic Y, Desbruyères D, Duarte CM, Rozenfeld AF, Bachraty C, Arnaud-Haond S (2012) Biogeography revisited with network theory: retracing the history of hydrothermal vent communities. Syst Biol 61:127–137

Nomaki H, Uejima Y, Ogawa NO, Yamane M and others (2019) Nutritional sources of meio- and macrofauna at hydrothermal vents and adjacent areas: natural-abundance radiocarbon and stable isotope analyses. Mar Ecol Prog Ser 622:49–65

Ogawa NO, Nagata T, Kitazato H, Ohkouchi N (2010) Ultrasensitive elemental analyzer/isotope ratio mass spectrometer for stable nitrogen and carbon isotope analyses. In: Ohkouchi N, Tayasu I, Koba K (eds) Earth, life, and isotopes. Kyoto University Press, Kyoto, p 339–353

Pereira OS, Shimabukuro M, Bernardino AF, Sumida PYG (2020) Molecular affinity of Southwest Atlantic *Alvinocaris muricola* with Atlantic Equatorial Belt populations. Deep Sea Res I 163:103343

Ponsard J, Cambon-Bonavita MA, Zbinden M, Lepoint G and others (2013) Inorganic carbon fixation by chemosynthetic ectosymbionts and nutritional transfers to the hydrothermal vent host-shrimp *Rimicaris exoculata*. ISME J 7:96–109

Portail M, Brandily C, Cathalot C, Colaço A and others (2018) Food-web complexity across hydrothermal vents on the Azores triple junction. Deep Sea Res I 131:101–120

Portanier E, Nicolle A, Rath W, Monnet L and others (2023) Coupling large-spatial scale larval dispersal modelling with barcoding to refine the amphi-Atlantic connectivity hypothesis in deep-sea seep mussels. Front Mar Sci 10: 1122124

Puillandre N, Brouillet S, Achaz G (2021) ASAP: assemble species by automatic partitioning. Mol Ecol Resour 21: 609–620

Reid WDK, Sweeting CJ, Wigham BD, Zwirglmaier K and others (2013) Spatial differences in East Scotia Ridge hydrothermal vent food webs: influences of chemistry, microbiology and predation on trophodynamics. PLOS ONE 8:e65553

Riekenberg PM, Carney RS, Fry B (2016) Trophic plasticity of the methanotrophic mussel *Bathymodiolus childressi* in the Gulf of Mexico. Mar Ecol Prog Ser 547:91–106

Rogers AD, Tyler PA, Connelly DP, Copley JT and others (2012) The discovery of new deep-sea hydrothermal vent communities in the Southern Ocean and implications for biogeography. PLOS Biol 10:e1001234

Rozas J, Ferrer-Mata A, Sanchez-DelBarrio JC, Guirao-Rico S, Librado P, Ramos-Onsins SE, Sanchez-Gracia A (2017) DnaSP 6: DNA sequence polymorphism analysis of large data sets. Mol Biol Evol 34:3299–3302

Schnabel KE, Peart RA, Bradford-Grieve J, Eagar S, Hosie A, Buckeridge J (2023) Kingdom Animalia, phylum Arthropoda, subphylum Crustacea (shrimps, crabs, lobsters, barnacles, & kin). In: Kelly M, Mills S, Terezow M, Sim-Smith C, Nelson W (eds) The marine biota of Aotearoa New Zealand: updating our marine biodiversity inventory. NIWA Biodiversity Memoir 136. NIWA, Wellington, p 411–445

Schoener TW (1974) Resource partitioning in ecological communities. Science 185:27–39

Stevens CJ, Limén H, Pond DW, Gélinas Y, Juniper SK (2008) Ontogenetic shifts in the trophic ecology of two alvinocaridid shrimp species at hydrothermal vents on the Mariana Arc, western Pacific Ocean. Mar Ecol Prog Ser 356:225–237

Stevens CJ, Juniper SK, Limén H, Pond DW, Metaxas A, Gélinas Y (2015) Obligate hydrothermal vent fauna at East Diamante submarine volcano (Mariana Arc) exploit photosynthetic and chemosynthetic carbon sources. Mar Ecol Prog Ser 525:25–39

Sun Y, Ogawa NO, Ishikawa NF, Blattmann TM, Takano Y, Ohkouchi N (2023) Application of a porous graphitic carbon column to carbon and nitrogen isotope analysis of underivatized individual amino acids using high-performance liquid chromatography coupled with elemental analyzer/isotope ratio mass spectrometry. Rapid Commun Mass Spectrom 37:e9602

Suzuki Y, Suzuki M, Tsuchida S, Takai K and others (2009) Molecular investigations of the stalked barnacle *Vulcanolepas osheai* and the epibiotic bacteria from the Brothers Caldera, Kermadec Arc, New Zealand. J Mar Biol Assoc UK 89:727–733

Sweetman AK, Levin LA, Rapp HT, Schander C (2013) Faunal trophic structure at hydrothermal vents on the southern Mohn's Ridge, Arctic Ocean. Mar Ecol Prog Ser 473: 115–131

Tajima F (1983) Evolutionary relationship of DNA sequences in finite populations. Genetics 105:437–460

Tayasu I, Hirasawa R, Ogawa NO, Ohkouchi N, Yamada K (2011) New organic reference materials for carbon- and nitrogen-stable isotope ratio measurements provided by Center for Ecological Research, Kyoto University, and Institute of Biogeosciences, Japan Agency for Marine-Earth Science and Technology. Limnology 12: 261–266

Teixeira S, Serrão EA, Arnaud-Haond S (2012) Panmixia in a fragmented and unstable environment: The hydrothermal shrimp *Rimicaris exoculata* disperses extensively along the Mid-Atlantic Ridge. PLOS ONE 7:e38521

Teixeira S, Olu K, Decker C, Cunha RL and others (2013) High connectivity across the fragmented chemosynthetic ecosystems of the deep Atlantic Equatorial Belt: efficient dispersal mechanisms or questionable endemism? Mol Ecol 22:4663–4680

Thomas EA, Sigwart JD, Helyar SJ (2022) New evidence for a cosmopolitan holothurian species at deep-sea reducing environments. Mar Biodivers 52:63

Tunnicliffe V, Breusing C (2022) Redescription of *Bathymodiolus septemdierum* Hashimoto and Okutani, 1994 (Bivalvia, Mytilida, Mytilidae), a mussel broadly distributed across hydrothermal vent locations in the western Pacific and Indian Oceans. Zootaxa 5214:337–364

Turco F, Ladroit Y, Watson SJ, Seabrook S and others (2022) Estimates of methane release from gas seeps at the Southern Hikurangi Margin, New Zealand. Front Earth Sci 10: 834047

Van Audenhaege L, Fariñas-Bermejo A, Schultz T, Van Dover CL (2019) An environmental baseline for food webs at deep-sea hydrothermal vents in Manus Basin (Papua New Guinea). Deep Sea Res I 148:88–99

Van Dover CL, Trask JL (2000) Diversity at deep-sea hydrothermal vent and intertidal mussel beds. Mar Ecol Prog Ser 195:169–178

Vereshchaka AL, Kulagin DN, Lunina AA (2015) Phylogeny and new classification of hydrothermal vent and seep shrimps of the family Alvinocarididae (Decapoda). PLOS ONE 10:e0129975

Webber WR (2004) A new species of *Alvinocaris* (Crustacea: Decapoda: Alvinocarididae) and new records of alvinocaridids from hydrothermal vents north of New Zealand. Zootaxa 444:1–26

Webber RW, Bruce NL (2002) Thriving blind — New Zealand's first volcanic vent shrimps. Biodivers Update 5:6–7

Webber RW, Fenwick GD, Bradford-grieve JM, Eagar SH and others (2010) Phylum Arthropoda, Subphylum Crustacea — shrimps, crabs, lobsters, barnacles, slaters, and kin. In: Gordon DP (ed) New Zealand inventory of biodiversity, Vol 2. Chaetognatha, Ecdysozoa, Ichnofossils. Canterbury University Press, Christchurch, p 98–232

Williams AB (1988) New marine decapod crustaceans from waters influenced by hydrothermal discharge, brine, and hydrocarbon seepage. Fish Bull 86:263–287

Williams AB, Chace FA (1982) A new caridean shrimp of the family Bresiliidae from thermal vents of the Galapagos Rift. J Crustac Biol 2:136–147

Williams AB, Dobbs FC (1995) A new genus and species of caridean shrimp (Crustacea: Decapoda: Bresiliidae) from hydrothermal vents on Loihi Seamount, Hawaii. Proc Biol Soc Wash 108:228–237

Williams AB, Rona PA (1986) Two new caridean shrimps from a hydrothermal field on the Mid Atlantic Ridge. J Crustac Biol 6:446–462

Wright IC, De Ronde CEJ, Faure K, Gamble JA (1998) Discovery of hydrothermal sulfide mineralization from southern Kermadec arc volcanoes (SW Pacific). Earth Planet Sci Lett 164:335–343

Yahagi T, Watanabe H, Kojima S, Beedessee G, Komai T (2014) First record and a new species of *Alvinocaris* Williams & Chace, 1982 (Crustacea: Decapoda: Caridea: Alvinocarididae) from the Indian Ocean. Zootaxa 3893: 101–113

Yahagi T, Watanabe H, Ishibashi JI, Kojima S (2015) Genetic population structure of four hydrothermal vent shrimp species (Alvinocarididae) in the Okinawa Trough, Northwest Pacific. Mar Ecol Prog Ser 529:159–169

Yaldwyn JC, Webber WR (2011) Annotated checklist of New Zealand Decapoda (Arthropoda: Crustacea). Tuhinga 22: 171–272

Yang CH, Tsang LM, Chu KH, Chan TY (2012) Complete mitogenome of the deep-sea hydrothermal vent shrimp *Alvinocaris chelys* Komai and Chan, 2010 (Decapoda: Caridea: Alvinocarididae). Mitochondrial DNA 23: 417–419

Zelnio KA, Hourdez S (2009) A new species of *Alvinocaris* (Crustacea: Decapoda: Caridea: Alvinocarididae) from hydrothermal vents at the Lau Basin, Southwest Pacific, and a key to the species of Alvinocarididae. Proc Biol Soc Wash 122:52–71

Zhou Y, Chen C, Zhang D, Wang Y and others (2022) Delineating biogeographic regions in Indian Ocean deep-sea vents and implications for conservation. Divers Distrib 28:2858–2870

Editorial responsibility: Philippe Borsa, Montpellier, France
Reviewed by: 3 anonymous referees

Submitted: November 8, 2023
Accepted: May 2, 2024
Proofs received from author(s): June 11, 2024